EXPLORING TIME DEPENDENT CHANGES TO SKELETAL MUSCLE MACROPHAGE REDOX HOMEOSTASIS IN A MODIFIED MOUSE MODEL OF EXPERIMENTAL AUTOIMMUNE MYOSITIS

ARSHDEEP THUHAN

A THESIS SUBMITTED TO

THE FACULTY OF GRADUATE STUDIES

IN PARTIAL FULFILLMENT OF THE REQUIREMENTS

FOR THE DEGREE OF

MASTER OF SCIENCE

GRADUATE PROGRAM IN KINESIOLOGY

YORK UNIVERSITY

TORONTO, ONTARIO

August 2023

Abstract

Myositis, a rare idiopathic inflammatory myopathy (IIM), is characterized by skeletal muscle wasting and weakness. While autoimmune-mediated, the etiology is largely unknown. The focus of this thesis was to assess a modified version of a model commonly used in the literature, known as experimental autoimmune myositis. We assessed the progression of this model over time in the gastrocnemius and soleus muscles, to explore muscle specific changes in the immune response. Our findings reveal changes to ROS production in muscle macrophages, as well alterations in the expression of inflammatory related genes. However, the modified model, with the absence of pertussis toxin, does not replicate the strong disease phenotype observed in traditional EAM models. This allows us to question the extent to which pertussis toxin induces a myositis phenotype as opposed to systemic inflammation. Ultimately, there is a need to develop a comprehensive model of myositis that accurately mimics the human condition.

Acknowledgements

First and foremost, I would like to thank both Dr. Christopher Perry and Dr. Ali Abdul-Sater for their continued support and insight over the last two years. I will always be grateful for all the patience you have had with my countless emails and follow-up emails . . . especially on weekends and holidays.

To Dr. Perry, thank you for all the science and life advice you have given me, and for listening to all my ramblings, particularly when I reveal huge life decisions in front of hot dog stands at conferences.

To the rest of my lab mates Cat, Shiv, Luca, Madison and Shahrzad, while I could never hear any of you the first time you'd say anything, I will always remember the jokes, random questions, and pink stained staircases. To Madison – thank you for being my right hand, and for pushing through to make this project come to life.

This thesis marks the end of an era for me, and I cannot even begin to count how many amazing experiences this lab and degree have given me, for which I will always be grateful.

Table of Contents

List of Tables

List of Figures

Chapter 1: Introduction

Myositis is a rare autoimmune disease, affecting between 14-17 per 100 000 people yearly in the United States[1]. With this disease, the immune system targets muscles, resulting in muscle weakness and fatigue[2]. Currently, there is no specific cause of myositis, but it is believed to arise following environmental triggers to the immune system. There are multiple known subcategories of myositis. The most widely known forms of myositis include polymyositis, dermatomyositis, inclusion body myositis, and immune mediated necrotizing myopathy. While the different forms of myositis present with largely similar symptoms, dermatomyositis is characterized by skin rashes or subcutaneous calcifications[2].

The immune system plays a large role in modulating disease. In myositis, many reports have found immune cell infiltration surrounding muscle fibers at the cellular level, implicating autoimmunity in the etiology of the disease. The presence of a variety of immune cells have been involved in the progression of myositis, including T and B lymphocytes, Natural Killer (NK) cells, macrophages, and more. In specific, macrophages play a large role in mediating an effective immune response. They are specialized immune cells that can recognize and phagocytose foreign pathogens in the body. Macrophages exhibit many cellular changes in response to pathogen recognition. Previous experiments have shown that one of these changes include an increase in mitochondrial reactive oxygen species (ROS) production[3]. Changes to macrophage ROS levels may play a crucial role in the immune response as downstream targets of ROS include the activation of various immune pathways[3].

The goal of this research is to modify a previously established mouse model of myositis, known as experimental autoimmune myositis (EAM)[4]. The EAM model is widely used by researchers, but it is not understood whether this model accurately reproduces the disease

phenotype. Currently, this model is induced by administering myosin protein combined with an adjuvant and pertussis toxin to mediate an immune response. However, the pertussis toxin may result in an overactive response, preventing us from studying the model over time[5]. Research done by Suzuki et al. (2005), showed that the EAM model can be induced without the use of the pertussis toxin[18]. However, this group used the SJL/J strain of mice, which express a dysferlin-deficiency and are susceptible to developing spontaneous myopathies[6]. Resultantly, we wanted to assess the robustness of the EAM model by evaluating whether it is inducible in wildtype mice, in the absence of pertussis toxin.

This model was assessed by determining changes to muscle-specific atrophy, weakness, and autoimmunity, through a time dependent model. In addition to this, macrophage characteristics were also assessed to elucidate any changes that may occur with the immune response over time. This included the identification of various immune cells and evaluating changes in macrophage mitochondrial (ROS) production and cellular oxidative stress. Ultimately, understanding the cellular mechanisms behind the EAM model can lead to a better understanding of how the human condition may be accurately modeled.

Chapter 2: Literature Review

2.1 Introduction to Myositis

2.1.1 Overview of Myositis and Subtypes

Myositis is an autoimmune mediated disease targeting muscle in the body and is commonly characterized as an idiopathic inflammatory myopathy (IIM). This rare disease most commonly presents as muscle weakness and fatigue in older populations, and primarily affects females. The reported annual prevalence of IIMs in the United States in 2012 was estimated at 14-17 per 100 000 people[1]. Currently, the exact mechanisms by which this disease develops is largely unknown. However, it is thought to be believed there may be multiple environmental or various other triggers that may prime the immune system to target the muscles, leading to inflammation. As such, patients are commonly prescribed with general corticosteroids or immunosuppressants to reduce inflammation, which may lead to adverse effects[7].

There are multiple subgroups of myositis, all of which are characterized as idiopathic inflammatory myopathies (IIMs). These include polymyositis (PM), inclusion body myositis (IBM), dermatomyositis (DM), and immune mediated necrotizing myopathy (IMNM)[2]. The different subtypes of myositis often present with similar symptoms of proximal muscle weakness. Commonly, in PM and DM, patients begin to experience muscle weakness and/or pain in the muscles of the arms and legs, which develops into a chronic condition. DM can be differentiated from PM through the presence of skin lesions or rashes, which are hallmark features of the subtype. IBM is often characterized by asymmetric muscle weakness, and commonly affects muscles involved in finger and ankle flexion[8]. Dysphagia, or difficult swallowing, is also common in IBM patients[9]. In addition to these physical manifestations of the disease subtypes, diagnosis requires further measures.

2.1.2 Clinical Manifestations and Diagnosis

As mentioned above, the different myositis subgroups exhibit similar symptoms of limb muscle weakness. Thus, an accurate diagnosis requires histological assessments of the muscle tissue and an antibody titer of myositis specific and/or myositis associated autoantibodies. Common symptoms observed in patients that lead to diagnosis include elevated serum levels of muscle enzymes (creatine kinase), and muscle histopathology such as the appearance of rimmed vacuoles and altered mitochondrial morphology[10]. In patients with DM, changes such as rashes, skin ulcers, and calcifications are also observed. These rashes are often characterized as a heliotrope rash (reddish rash covering the eyelids), gottron's papules (rash/bumps over the back of the knuckles), and/or hyperkeratosis in the hands[11]. IBM is characterized by elevated protein aggregates, consisting of amyloid precursor protein, β-amyloid, and other proteins. These protein aggregations are similar to those observed in Alzheimer's disease[12]. Additionally, myositis patients may present symptoms in addition to other conditions. Interstitial lung disease is often diagnosed in patients with PM or DM[13]. The presence of myositis specific autoantibodies in patient serum are also used to characterize specific subgroups to ensure an accurate diagnosis. While there are multiple autoantibodies that overlap between myositis subgroups, the most commonly found antibody in both PM and DM is anti-histidyl tRNA synthetase (Anti-Jo1). Additionally, the anti-signal recognition particle (SRP) antibody has been found to be specific to PM and IMNM patients, while Anti-Mi2 is specific to DM patients, and is associated with the presence of skin conditions[14]. In IMNM, the presence of Anti-SRP and/or anti-hydroxy-3-methylglutaryl-CoA reductase (anti-HMGCR) are associated with severe muscle weakness[15]. While these myopathies can be difficult to diagnose, using a range of assessments at various whole body and cellular levels can provide an accurate diagnosis for patients.

2.1.3 Experimental Autoimmune Myositis

While multiple models of myositis are being used by researchers, the experimental autoimmune myositis (EAM) model is one of the most widely used murine models of myositis. Briefly, the induction of this model involves multiple weekly injections of a foreign myosin protein (e.g. rabbit), which acts as an antigen, along with an adjuvant to stimulate an immune response against the antigen. The adjuvant used most often is Freund's complete adjuvant (CFA), which contains mycobacteria[16]. Other adjuvants tested in this model have included Alum and CpG, which were not successful in the induction of EAM[17]. Researchers using this model often use the SJL/J or BALB/c strain of mice. The SJL/J strain presents with a dysferlinopathy, which leads to spontaneous muscle weakness[7]. Dysferlin is a sarcolemmal protein which plays a role in membrane repair and stability following damage[7]. With this strain, EAM induction is likely to occur as the mice are more prone to myopathy[18]. On the other hand, BALB/c mice are a wildtype strain and do not normally develop any spontaneous myopathy without an intervention. Currently in the literature, researchers that have utilized this strain of mice include an injection of pertussis toxin in conjunction with the myosin and adjuvant to allow for a stronger immune response to occur[17]. Pertussis toxin is an exotoxin secreted by *Bordatella pertussis.* As it's mechanism of action, this toxin can inhibit the α subunit of G proteins, leading to downstream disruptions in G protein coupled signalling, as well as increased cyclic adenosine monophosphate (cAMP) signalling. These alterations to cell signalling processes have been associated with increased activation of immune cells, as well as increased cytokine production for a stronger immune response[66]. As a result, using pertussis toxin as an adjuvant can create a stronger reaction against the foreign myosin protein and lead to muscle weakness. However, there is a gap in the literature that delineates the induction of EAM from a whole-body immune

response to the strong adjuvants/toxins that are used. Previous research assessing this model hypothesized animal death during observation to be a result of multiple organ failure derived from exposure to strong toxins at multiple time points[19]. In order to accurately replicate the human myositis condition, a suitable model that does not require the use of extreme toxins should be developed. Additionally, no research to our knowledge exists that involves the induction of this model without requiring continuous immunizations in a wildtype mouse strain to maintain the phenotype.

2.1.4 C-protein Induced Myositis

C-protein induced myositis (CIM) is another model used to replicate the human condition in a murine model. This model involves the introduction of c protein, a myosin-binding protein found in muscle tissue, with CFA and pertussis toxin[16]. While this model does not require repeated immunizations, previous research has been unable to show the induction of CIM without the use of both CFA and pertussis toxin[20]. For this reason, this model is similar to the EAM model.

A modified model of CIM has also been used to induce myositis in mice. This model is characterized by the injection of bone marrow derived dendritic cells (BMDCs) pulsed with a c protein fragment peptide (as opposed to larger c protein fragments), alongside CFA, to induce a response. In this model, the myositis phenotype, characterized by immune cell infiltration around muscle fibers, was induced 7 days after the transfer of cells. This model has shown to be extremely transient, as the myositis phenotype disappears after the first 14 days following disease induction[21]. Thus, continuous immunizations are required to maintain and study the disease phenotype.

2.2 Overview of Mechanisms of Autoimmunity

2.2.1 Introduction to the Immune System

The immune system is often characterized as a two-armed response to a stressor – the innate and adaptive responses. The innate immune response may begin to act within hours or days of an immune attack, whereas the adaptive response may take up to 1-2 weeks[22]. Generally, the innate immune system is the first to respond to pathogens and exerts a broad response. The adaptive response, on the other hand, generates a more robust, antigen specific response to target the invading pathogen(s). Adaptive immunity is characterized by the activation of lymphocytes (T cells and B cells) in response to the stressor[22]. Beyond anatomic barriers such as epithelial layers, the primary cells involved in the innate immune response include granulocytes (such as basophils and eosinophils) as well as phagocytic cells (such as dendritic cells and monocytes/macrophages)[23]. Inflammatory cytokines also accumulate at areas of invasion to positively regulate the activation and recruitment of other immune cells[24]. Innate immune cells are also involved in the activation of the adaptive immune response, as shown in Figure 1 below. Specifically, dendritic cells and macrophages (innate immune cells) possess the ability to phagocytose the foreign pathogen and present it to T cells as part of lymphocyte activation[22]. Macrophages can also mediate a spectrum of responses, depending on the subtype, which is further discussed in the following section. Upon activation, T cells may be involved in two distinct mechanisms. T helper cells (T_h cells) aid in further mediating the immune response by producing cytokines to promote the activation of various other immune cells. On the other hand, cytotoxic T cells can induce apoptosis of foreign cells[24]. T cell responses also involve further activation of macrophages through the production and release of specific interferons[22]. Thus, the two branches of the immune system have interconnected roles in order to mediate an effective

response. The other major cell type involved in the adaptive immune response are B lymphocytes, which can be activated by T_h cells. The primary role of B cells is to mediate the humoral response by producing antibodies that are specific to the antigen invading the body[24]. This specific response allows for a more robust attack against the invading pathogen and provides 'memory' for future attacks from the same pathogen.

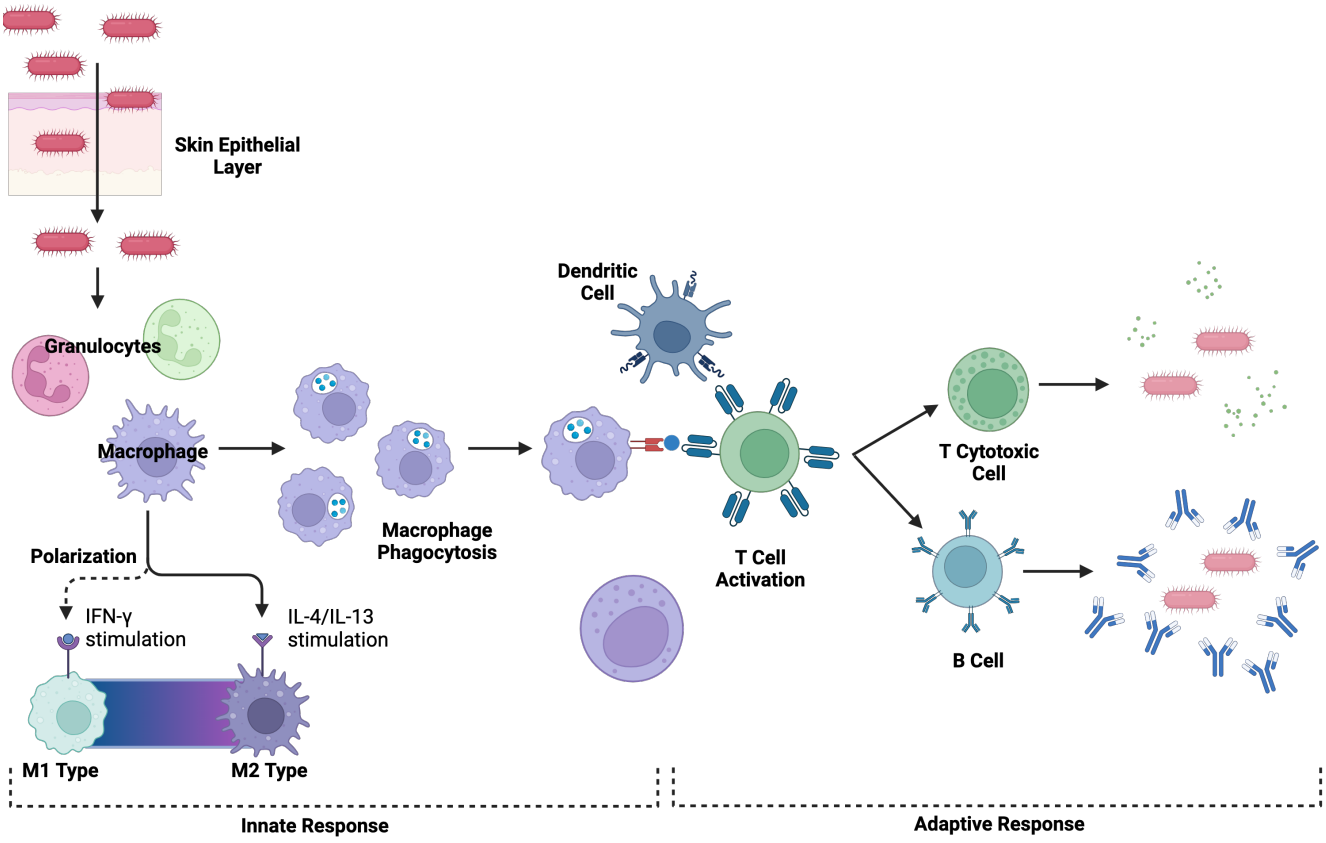

Figure 1: Overview of the two branches of the immune response.

A simplified overview of the events following pathogen (in red) detection. A broad categorization of cells involved in the innate and adaptive responses are shown. Created using Biorender, 2023.

2.2.2 Macrophage Biology

Macrophages are known to play a crucial role in both innate and adaptive immunity. They primarily use phagocytosis to remove foreign antigens[25]. Macrophages mediate their responses

following activation, which may include signals produced by other innate immune cells during the primary response to an antigen[26]. Common myeloid progenitor cells can form monocytes, which then differentiate into mature macrophages in response to pathogens[27]. Classically, macrophages are characterized according to their response. While more complex subgroups are now being studied, the most common form of classification includes the M1 and M2 macrophage subtypes. During an immune response, macrophages may exhibit a range of functional subtypes, between the pro and anti-inflammatory extremes[28].

In terms of the simplified M1/M2 dichotomy, macrophage polarization will direct the response that is observed. Generally, M1 macrophages are associated with pro-inflammatory responses, whereas M2 macrophages exhibit an anti-inflammatory response. The metabolic changes involved in the process of macrophage polarization are discussed in more detail in section 2.4. M1 macrophages are referred to as classically activated, while M2 macrophages are alternatively activated. Classical activation is mediated by IFN-γ, which is a cytokine produced by immune cells, such as T helper (T_h1) cells. Following binding of IFN-γ to its receptor on macrophage cell membranes, downstream transcription factors are activated, leading to the transcription of genes involved in mediating a pro-inflammatory immune response, such as cytokines and phagocytic receptors[29]. Alternative activation occurs following the binding of IL-4 or IL-13, produced by T_h2 cells or other innate immune cells, to the macrophage IL-4Rα1 and IL-13Rα1 receptors, respectively. Again, downstream cellular pathways are activated, to promote the upregulation of genes involved in anti-inflammatory responses and tissue repair[30]. Differences between M1 and M2 macrophages include the production of various factors/cytokines as well as surface receptor expression[31]. While F480 is used as a general macrophage marker, M1 and M2 subtypes express different receptors following polarization.

Additionally, M1 macrophages often produce pro-inflammatory factors as part of their response, such as IL-6 and IL-1β [31]. On the other hand, M2 macrophages express increased IL-10, and TGF-β (among others), to aid in tissue repair and healing[32].

2.2.3 Muscle Resident Macrophages

Tissue specific macrophages play important roles in mediating location dependent immune responses. In many tissues, macrophages have adapted to perform functions specific to that location. Muscle resident macrophages are involved in the repair of muscle tissue following injury and exercise in order to maintain tissue homeostasis[33]. At different stages during tissue repair, macrophages can exhibit varied levels of polarization to aid in their response. During resting states, resident muscle macrophages have shown to be polarized more towards the anti-inflammatory, or M2-like state. This was marked by the presence of CD206, a receptor specific to M2-like macrophages[34]. Research conducted by Krasniewski et al. (2022) assessed macrophage subpopulations in skeletal muscle tissue. These subpopulations contained markers associated with a variety of both pro and anti-inflammatory functions, such as proliferation, repair, and a range of phagocytic activity. They also reported increases in pro-inflammatory macrophage markers in aged skeletal muscle, further supporting the heterogeneity and plasticity of macrophages[34].

However, dysregulation of immune signaling and macrophage function may lead to a diseased state. Research in the field of muscular dystrophies has shown that both pro- and anti-inflammatory macrophages are elevated in muscle tissue, which may be contributing to exaggerated inflammation and increased fibrosis[35]. In human myositis muscle, the presence of both pro- and anti-inflammatory macrophages has also been characterized[36]. Additionally, increases in inducible nitric oxide synthase (iNOS) have been reported[36]. iNOS is associated with

increases in nitric oxide (NO) production, which aids in the pro-inflammatory response by promoting vasodilation for movement of immune cells and the production of inflammatory mediators[37]. The expression of TGF-B, an anti-inflammatory mediator, in areas of severe immune infiltration and muscle damage has also been reported[36]. This may be a result of a compensatory mechanism in attempt to reduce damage sustained by pro-inflammatory responses. These dysregulated responses may be leading to the disease phenotype observed in myositis and may vary according to the type of inflammatory myopathy observed.

2.3 Overview of Mitochondrial Respiration and ROS production

2.3.1 Overview of Mitochondrial Respiration

The mitochondrion, often referred to as the energy powerhouse of the cell, plays a crucial role in cellular metabolism. Mitochondrial structure consists of two membranes, referred to as the inner mitochondrial membrane (IMM) and outer mitochondrial membrane (OMM), between which exists the intermembrane space (IMS). Energy carried in the form of adenosine triphosphate (ATP) is used by cells in various physiological cascades required for cellular function. Briefly, this process begins with the consumption of sugars, or carbohydrates, that are converted into pyruvate molecules through glycolysis in the cell cytoplasm[38]. Glycolysis also provides metabolic intermediates for a parallel pathway, known as the pentose phosphate pathway (PPP). This pathway is used to produce electron carriers and amino acid precursors, that will be used by the cell to meet physiological demands[28]. The pyruvate molecules produced through glycolysis are shuttled into the inner mitochondrial matrix, where they are converted to acetyl-coA, by the pyruvate dehydrogenase complex, linking glycolysis to the next step. Acetyl-coA will flux through the tricarboxylic acid (TCA) cycle, during which nicotinamide adenine

dinucleotide (NAD^+) and flavin adenine dinucleotide (FADH) are reduced, producing carbon dioxide (CO_2) in the process. These electron carriers, known as NADH and $FADH_2$, supply the electron transport chain (ETC) with electrons, which ultimately relies on the movement of electrons through four complexes and the generation of a proton gradient, to produce ATP through the phosphorylation of adenosine diphosphate (ADP), as shown in Figure 2. Oxygen (O_2) is consumed in this process; thus, it is referred to as oxidative phosphorylation[38] and will be described in more detail in the next section. The processes of both glycolysis and the ETC catalyze the conversion of ADP to ATP. One molecule of glucose generates two molecules of ATP through glycolysis, while the ETC may generate 30-32 molecules of ATP. While the ETC provides cells with more molecules of ATP, the process of glycolysis can lead to the production of more metabolic intermediates and precursors for protein synthesis[28]. The physiological relevance of these processes in states of disease is important in assessing the role of mitochondrial dysfunction.

2.3.2 Electron Transport Chain

Embedded within the IMM, the ETC provides the most crucial process for oxidative phosphorylation and ATP production[39]. Electrons donated through NADH and $FADH_2$ carriers move through four complexes, known as NADH-ubiquinone oxidoreductase (complex I), succinate dehydrogenase (complex II), cytochrome bc_1 complex (complex III), and cytochrome c oxidase (complex IV), which precede phosphorylation of ADP at ATP synthase (complex V), as represented in Figure 2. Complex II also plays a role in the tricarboxylic acid (TCA) cycle, as it mediates the conversion of succinate to fumarate during step 6 of the cycle (Figure 4). The transfer of electrons through complexes I-IV via transfer carriers known as ubiquinone and cytochrome c, drives the movement of protons (H^+) from the inner mitochondrial matrix into the

intermembrane space, generating a strong electrochemical gradient. The movement of electrons is coupled with the movement of protons. Each successive protein complex exhibits increasing affinity for electrons, allowing them to be pulled forward sequentially through the ETC. At complex IV, the electrons are donated to O_2, also known as the final, highest affinity electron acceptor, generating H_2O in the process[39]. The proton gradient is dissipated when protons return to the matrix by moving through ATP synthase, allowing the complex to catalyze the phosphorylation of ADP using inorganic phosphate (P_i), to ATP, for the cell to use as energy[40].

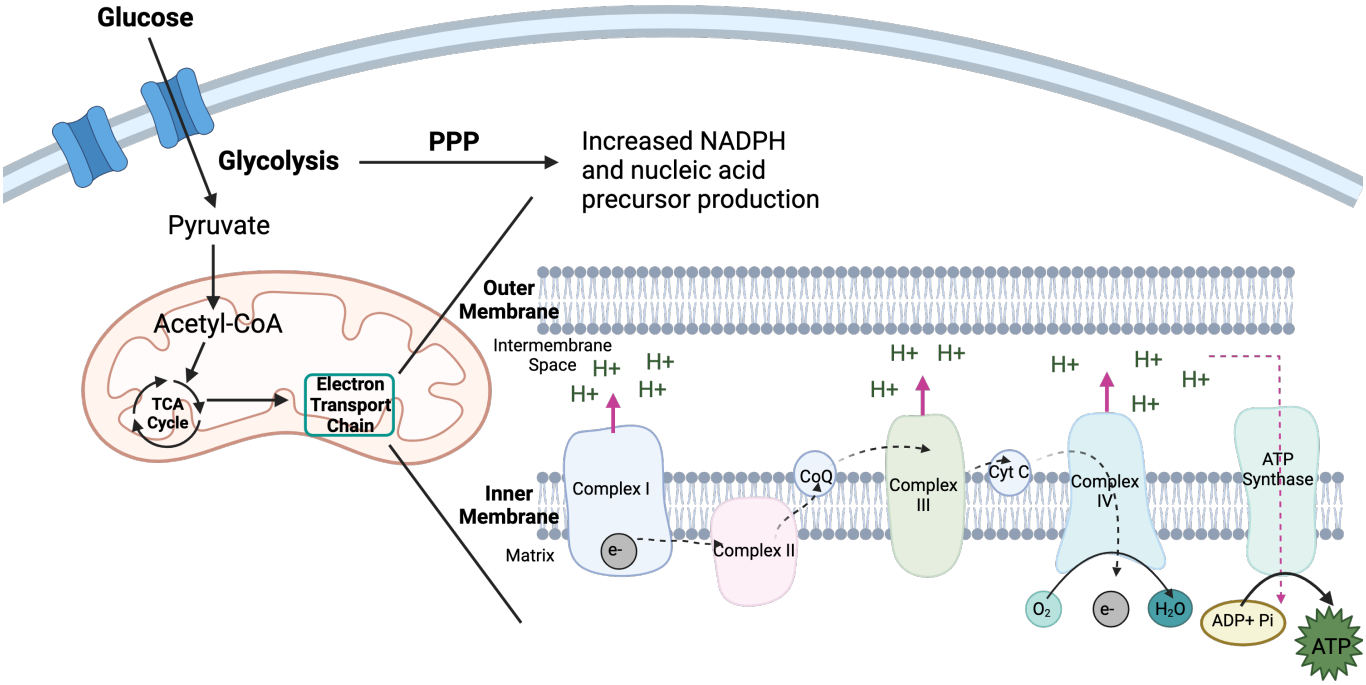

Figure 2: Overview of mitochondrial respiration.

The processes involved in mitochondrial respiration are shown in cytosolic and mitochondrial compartments. The electron transport chain is enlarged to depict the details that are involved. Created using Biorender, 2023.PPP: Pentose Phosphate Pathway; TCA Cycle: Tricarboxylic Acid Cycle; CoQ: Coenzyme Q; Cyt C: Cytochrome C.

2.3.3 ROS Generation and Cellular Defenses

The electron transport chain requires the movement of electrons to power ATP production. However, if electrons are unable to move forward, they can be transferred prematurely to O_2, generating $O_2^{\bullet -}$ (ROS-superoxide)[40], a phenomenon known as electron slip. Cells have adapted to develop mechanisms to protect themselves against excess oxidative stress/damage, to a certain extent. Superoxide dismutase (SOD) has the ability to reduce mitochondrial superoxide to hydrogen peroxide (H_2O_2), which can diffuse out of the mitochondria. In the cell cytoplasm, catalase can then convert H_2O_2 into H_2O, to neutralize ROS[41]. Cells also use antioxidant systems to limit excess ROS accumulation. One of these includes the glutathione (GSH) system[42]. This process is represented in Figure 3 below. Structurally, glutathione is a tripeptide, composed of glutamic acid, cysteine, and glycine. Glutathione contains a thiol (S-H) group, in the form of the cysteine residue. Upon oxidation, two oxidized glutathione molecules will form a disulfide bond, to create GSSG[43]. In response to oxidative stress, glutathione peroxidase (GPx) uses GSH to neutralize H_2O_2 into H_2O, forming GSSG in the process. The ratio of reduced (GSH) to oxidized (GSSG) glutathione is crucial in maintaining homeostasis. Under resting conditions, mammalian cells usually express a GSH:GSSG ratio of 100:10, which may decrease to 10:1 during periods of oxidative stress[44]. Cells can regenerate GSH using gluthathione reductase (GR), which uses NADPH to mediate the conversion of GSSG to GSH[42]. Other antioxidant systems include the thioredoxin and peroxiredoxin systems, which employ similar mechanisms as the glutathione system to neutralize ROS[41].

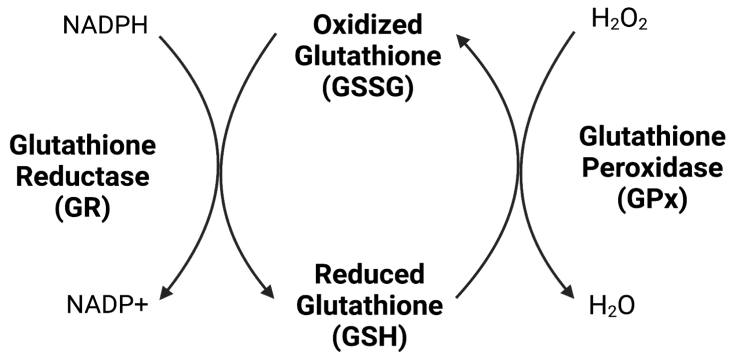

Figure 3: Cellular glutathione buffering system.

The relationship between oxidation and reduction of glutathione through the actions of glutathione peroxidase (GPx) and glutathione reductase (GR) are shown. This system aids in neutralizing excess levels of hydrogen peroxide (H_2O_2). Created using Biorender, 2023.

2.4 Immunometabolic Regulation of Macrophages

2.4.1 Changes to Macrophage Mitochondrial Metabolism

During the process of immune cell activation, macrophages have been shown to use metabolic shifts to mediate responses and aid in polarization[45]. As described earlier, macrophage polarization is often characterized by a shift on the spectrum of anti- or pro-inflammatory phenotypes, the degree to which can vary. This polarization involves the expression of different metabolic and inflammatory mediators to maintain their respective functions. M1, or pro-inflammatory macrophages, have been shown to rely on glycolysis as their primary source of energy. M2 (anti-inflammatory) macrophages, on the other hand, shift toward increased (OXPHOS)[45]. The process of this metabolic shift, or, glycolytic switch, involves alterations in the expression of genes involved in metabolism. This change has been well characterized in cancer cells and is referred to as the Warburg Effect[46]. In macrophages, similar metabolic alterations are also observed. Glycolytic shifts and increased glucose uptake have been implicated in mediating a pro-inflammatory immune response and are associated with increased

expression of inflammatory cytokines and mediators[47]. Shifting towards glycolytic flux and increased use of the pentose phosphate pathway might help meet cellular demands for proliferation and function by providing metabolites required for these processes. For instance, increased glycolysis can increase the use of the PPP, which can replenish NADPH required for mediating an immune response using NADPH oxidases (further discussed in the next section). In response to activation stimuli, M1 macrophages experience an interrupted TCA cycle, resulting in the accumulation of metabolic intermediates, shown in Figure 4 below. These include citrate, succinate, and itaconate[28]. These intermediates have a role in mediating downstream changes that further encourage a glycolytic reliant environment. Briefly, accumulation of citrate has the potential to promote production of reactive oxygen species (ROS)[48]. Citrate is moved into the cell cytoplasm through the mitochondrial citrate carrier (CIC), the expression of which has also shown to be upregulated in pro-inflammatory responses[49]. Cytosolic citrate can be converted into acetyl-CoA and oxaloacetate, which plays a role in downstream production of ROS and inflammatory mediators[50]. Increased itaconate has shown to inhibit the ETC complex SDH by competitively blocking the enzyme's active site[51]. Normally, SDH oxidizes succinate into fumarate as part of the TCA cycle[28]. Inhibition of SDH results in increased levels of succinate. Elevated succinate, in conjunction with an interrupted TCA cycle and reduced OXPHOS can lead to increased levels of ROS, the effects of which will be discussed in the following section[28].

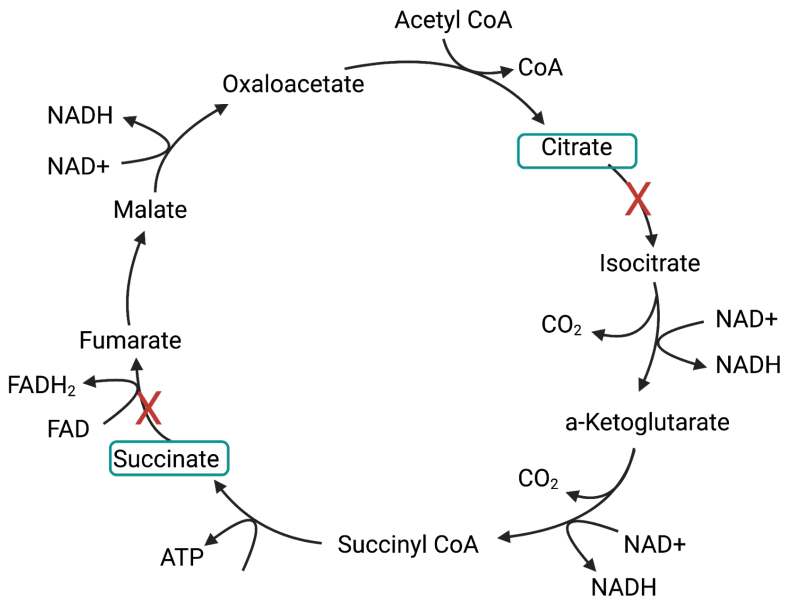

Figure 4: Interrupted TCA cycle during glycolytic shifts.

Overview of the tricarboxylic acid (TCA) acid and metabolites that are released. During immunometabolic shifts, the cycle is interrupted at two stages, represented as a red 'X'. Created using Biorender, 2023.

2.4.2 Reactive Oxygen Species in Immunity

Macrophage reactive oxygen species production has been linked to effective phagocytosis of apoptotic or damaged cells. The two most common sources of ROS include NADPH oxidases (NOXs), and mitochondria[52]. NADPH oxidases, normally located on cell plasma membranes, produce large amounts of superoxide for the process of respiratory burst, leading to effective pathogen clearing. The phosphorylation of cytosolic components leads to translocation to the plasma membrane, forming the larger NADPH oxidase enzyme complex. Cytosolic NADPH is consumed in the process of reducing O_2 for production of ROS in the form of $O_2^{\bullet-}$. In addition to pathogen killing, NADPH oxidase activation can promote downstream signaling pathways that ultimately aid in pro-inflammatory responses, such as the NF-κB pathway. Superoxide produced by NADPH oxidase is converted to H_2O_2 (as described in Section 2.3.3), which can lead to

activation and nuclear recruitment of the regulator NF-κB. Resultantly, pro-inflammatory related genes can be upregulated, such as those encoding pro-inflammatory cytokines to maintain the immune response[53]. Mitochondria also provide an important source of ROS for immune cells. Mitochondrial ROS production has been linked to the activation of various downstream effectors that lead to increased expression of pro-inflammatory genes[54]. One mechanism that leads to these changes is the activation of hypoxia-inducible transcription factor 1 alpha (HIF1α)[55], which is involved in cell adaptations to hypoxic environments[56]. As a result, a pseudo-hypoxic environment is created in the cells. Excess ROS can promote inhibition of SDH, which, as discussed in the previous section, can lead to elevated succinate levels. Succinate is an important metabolite as it can also support increased stabilization of HIF1α. Under normoxic conditions, HIF1α is degraded by prolyl hydroxylases (PHDs). However, during a pro-inflammatory response, an increased presence of cytosolic succinate can diminish PHD activity, ultimately allowing for increased HIF1α stabilization. HIF1α translocates into the nucleus and can lead to the expression of various genes to promote a glycolytic shift (as observed in M1/pro-inflammatory macrophages), through the upregulation of glucose transporters (GLUTs), and the inhibition of enzymes involved advancing the TCA cycle and ETC[57]. This further supports a reduction in OXPHOS and promotes glycolysis and PPP in cells[58]. Again, glycolysis and the PPP provide metabolites such as NADPH to help power NADPH oxidase ROS production. These interconnected processes allow for faster generation of metabolites required to meet the demands of the pro-inflammatory macrophages, and to mediate effective responses.

Chapter 3: Rationale and Hypothesis

3.1 Rationale

The use of the EAM model has been the standard in myositis research. However, to accurately depict the human condition, the model must be understood at a deeper level. Currently, in the literature, EAM is induced by introducing a foreign myosin protein with a strong adjuvant (complete Freund's adjuvant-CFA) to stimulate an immune response. Researchers that have used wildtype mice (BALB/c) also inject pertussis toxin (PT) in order to ensure a strong response is established. In experiments that have avoided the use of PT, mice that are prone to developing spontaneous myopathies are used. The SJL/J strain of mice have a dysferlin mutation, which normally plays a role in muscle sarcolemma repair following damage. As a result, these mice are more likely to exhibit the EAM phenotype without the use of PT. However, it is possible that the combination of CFA and PT in injections may result in an excessive immune reaction, affecting other organs and body systems in addition to the muscle. The use of the EAM model, to our knowledge, has not been induced in wildtype mice without the use of strong adjuvants and toxins, thus it does not effectively replicate the human condition. Furthermore, this model requires weekly injections, suggesting that the phenotype may be transient, challenging the effectiveness of this model. Therefore, to understand the robustness of the model, and to assess whether a response against the myosin protein can be induced without stimulating an extreme autoimmune response, we used a time course model to evaluate the effect of successive immunizations in a modified model of EAM using wildtype (BALB/c) mice, without pertussis toxin.

Mitochondrial dysfunction and immune cell infiltration at the whole muscle level have been established in the EAM model[59]. Additionally, the role of the immune system as a whole and

potential immune mechanisms and cellular cascades have been hypothesized in the development of human myositis, although the exact cause of the disease is largely unknown. In other disease models, such as cancer[46] and Duchenne's Muscular Dystrophy[35], the role and differentiation of macrophages at a deeper, cellular level have also been assessed. However, in the EAM model, this remains yet to be elucidated. Assessing the role of the initial innate immune response through macrophage characteristics and activation in a muscle specific manner may aid in a more extensive understanding of this current model, and the development of a more suitable disease model.

3.2 Objectives

This project assessed the time dependent and muscle specific changes in the EAM model, through assessments conducted at the whole body and cellular levels. The specific objectives were as follows:

(1) To assess the induction of a modified EAM model in wildtype (BALB/c) mice in the absence of pertussis toxin.

(2) To determine the degree of muscle wasting and/or atrophy associated with the progression of the modified EAM model at the functional and cellular levels.

(3) To assess the changes in immune cell characteristics and infiltration in two muscle tissues (gastrocnemius and soleus).

3.3 Hypothesis

We hypothesize that a decline in muscle health will be observed as the number of injections increase, but the phenotype will be improved during phase 3, after injections are halted. We also

hypothesize that an initial inflammatory response will be exhibited, with levels of infiltrating immune cells decreasing over time (in phase 3).

3.4 Author contributions

The experiments outlined in this thesis were conducted by Arshdeep Thuhan (AT) and Madison Garibotti (MG). All animal assessments and monitoring, anthropometric measurements, tissue preparations, and analyses were performed by AT and MG. Tissue collections and surgeries were aided by Shahrzad Khajehzadehshoushtar (SK) and Luca Delfinis (LD).

3.5 Additional contributions

The following list comprises the additional contributions I have made during my MSc that are not included in this thesis:

Co-author published:

Bellissimo C.A., Gandhi S., Castellani L.N., Murugathasan M., Delfinis L.J., **Thuhan A.K.**, Garibotti M.C., Seo Y., Rebalka I.A., Sweeny G., Hawke T.J., Abdul-Sater A.A., Perry C.G.R. (2023). Adiponectin receptor agonism attenuates fibrosis, inflammation and mitochondrial H_2O_2 emission in diaphragm from the D2.*mdx* mouse model of Duchenne muscular dystrophy. In review, *FASEB J.* doi: https://doi.org/10.1101/2023.05.22.541826

Delfinis L.J., Bellissimo C.A., Gandhi S., DiBenedetto S.N., Garibotti M.C., **Thuhan A.K.**, Tsitkanou S., Rosa-Caldwell M.E., Rahman F.A., Cheng A.J., Wiggs M.P., Schlattner U., Quadrilatero J., Greene N.P., Perry C.G.R. (2022). Muscle weakness precedes atrophy

during cancer cachexia and is linked to muscle-specific mitochondrial stress. *JCI Insight*. 7(24):e155147.

Co-author in progress:

Delfinis L.J., Gandhi S., Garibotti M.C., **Thuhan A.K.**, Reid R.A., Khajehzadehshoushtar S., Ogilvie L.M., Matuszewska K., Periera M., Cheng A.J., Simpson J.A., Petrik J. and Perry C.G.R. (2021). Muscle mitochondrial pyruvate oxidation is reduced in early-stage ovarian cancer but partially restored in advanced-stage.

Garibotti M.C., **Thuhan A.K.**, Delfinis L.J., Khajehzadehshoushtar S., Abdul-Sater A.A., and Perry C.G.R. (2023). Examining the relationship between mitochondrial stress and muscle health in a modified mouse model of experimental autoimmune myositis.

Chapter 4: Materials and Methods

4.1 Animal Care

10-16 week old female BALB/c mice were purchased from Envigo and provided access to standard chow and water ad libitum. Females were used since myositis is more prevalent in the female population[1]. Mice were allowed to acclimatize for a minimum of 7 days prior to handling and immunizations. All experiments and procedures were approved by the York University Animal Care Committee (AUP Number 2019-17) in accordance with the Canadian Council on Animal Care. Animals were monitored daily for changes in body weight, well-being, and skin lesions.

4.2 Myosin and Adjuvant Injections

4.2.1 Myosin Purification

Myosin was purified from rabbit skeletal muscle using a protocol provided by Dr. Leslie Leinwand at the University of Colorado (Appendix A). Freshly sacrificed rabbits were obtained from a commercial food supplier (Abate packers, Arthur, ON) which meets Canadian Health requirements for the ethical treatment of animals, and hindlimb and forelimb skeletal muscle tissue was collected for purification. The myosin was stored in 50% glycerol at -20°C. Myosin purity was assessed using a Coomassie Blue gel protein stain (Supplemental 1). Bands were identified using previous literature and included trace sarcomeric proteins. The purified myosin concentration was calculated to be 4.203 mg/mL using a standard Bradford Assay.

4.2.2 Coomassie Blue Stain

Myosin purity was assessed using a Coomassie Blue gel stain. 0.5-1 ug/uL of denatured and reduced protein was subject to a 4-12% gradient polyacrylamide gel. The gel underwent a fixing

procedure for 60 minutes at room temperature using an isopropanol based fixing solution of 25% isopropanol, 10% acetic acid, and 65% H_2O. Following this, rapid Coomassie blue staining solution (10% acetic acid, 0.006% Coomassie Brilliant Blue G-250, BioRAD, 90% H_2O) was used to cover the gel, and was rotated gently overnight, at room temperature. The next day, the gel was covered in 10% acetic acid for two hours, to destain. The gel was imaged using an iPhone camera, and bands were qualitatively assessed.

4.2.3 Inoculation Procedure

The inoculation procedure was based on previous literature[17, 59] with certain modifications. Specifically, pertussis toxin injections were not included in order to determine the effects of myosin and adjuvant combinations. Mice received inoculations of myosin emulsified with an adjuvant to enhance the immune response. The primary immunization consisted of purified rabbit myosin in glycerol mixed with Freund's Complete Adjuvant (CFA) (Sigma) and subsequent injections used Freund's Incomplete Adjuvant (IFA) (Sigma). CFA contains 1 mg/mL of heat killed *Mycobacterium tuberculosis* to stimulate the immune system.

Mice were inoculated every 7 days, corresponding to their experimental group as explained in the following section. Injections were administered subcutaneously at 4 sites, with 2 located below each shoulder blade, and two at both flanks. The volume of the injection emulsification was calculated using previous research done by Suzuki et al. (2005), who injected 1.32 mg of myosin per site[18]. In order to replicate this, each injection site was given 78.5 uL of the emulsion.

4.2.4 Experimental Groups

Three phases were included in this time course study, with three experimental groups per phase. The experimental groups were as follows:

Modified-EAM/Myosin group (M): Received 50% myosin+glycerol with 50% CFA/IFA

CFA/IFA Control Group (GCI): Received 50% glycerol with 50% CFA/IFA

Glycerol Control Group (GS): Received 50% glycerol with 50% saline

Phase 1 (n=8) consisted of three weekly injections, with tissue collection/sacrifice 7 days following the final injection. Phase 2 (n=12) involved four sets of weekly injections with sacrifice 7 days following the last immunization. Phase 3 (n=8) consisted of four weekly injections with sacrifice scheduled 28 days after the final injection (Figure 5A).

4.3 Tissue Collection/ Surgery Procedure

Following each tissue collection, the quadriceps, tibialis anterior (TA), extensor digitorum longus (EDL), liver, kidney, spleen, and adipose tissue were collected under isoflurane anesthesia prior to euthanasia. These tissues were snap frozen in liquid nitrogen and stored at -80°C. The gastrocnemius and soleus muscles were weighed and placed in a phosphate buffered saline (PBS) solution to use for flow cytometric analyses. The muscles of the second hindlimb and diaphragm were frozen and embedded in optimal cutting temperature (OCT) medium using liquid nitrogen chilled isopentane and stored at -80°C.

4.4 Functional Analyses

4.4.1 Grip Strength

Forelimb grip strength was assessed as reported previously. Briefly, using a metal grid attached to a force transducer to record peak tension. Three trials were recorded in total, and the mice were allowed 30-45 seconds of rest between each trial. The maximum peak tension was used for analysis. Grip strength measurements were recorded on the date of tissue collection.

4.4.2 Cage Hang Time

Cage hang time was assessed by placing the animal on a metal cage top and inverting it approximately 35 cm above an empty padded cage. The maximum time allocated per trial was three minutes, after which no more trials were conducted. If the animal held on for less than three minutes, an additional trial was conducted, for a total of three attempts with 30-45 seconds of rest between trials. The longest attempt was used for analysis and measurements were recorded on the date of tissue collection.

4.5 Histological Assessments

4.5.1 Hematoxylin and Eosin (H&E) Staining

Histological procedures included hematoxylin and eosin staining on 8 um sections of OCT compound embedded gastrocnemius and soleus muscles.

For the staining procedure, hematoxylin stain was added to cover samples on each slide for 30 seconds. Following this, the slides were gently rinsed using warm tap water and then stained with eosin for 5 minutes. Next, the sections underwent a dehydration process using three 70%-99% ethanol washes. The slides were then submerged in xylene and a mounting medium was added to secure a cover slip onto the slide. The stained samples were imaged using the EVOS Imager and were assessed for areas of immune cell infiltration (expressed as a % of the entire muscle section) using the Image J software.

4.5.2 Myosin Heavy Chain (MHC) Staining

To allow for the assessment of muscle fiber type-specific atrophy within these samples, the muscle tissue was embedded and cut as previously explained and stained with myosin heavy chain-specific antibodies. Slides were air-dried for 5-10 minutes then blocked with goat serum in

PBS for an hour at room temperature. All primary antibodies were purchased from the Developmental Studies Hybridoma Bank (University of Iowa), and secondary antibodies were purchased from Invitrogen. Slides were incubated with primary antibodies against myosin heavy chain MHCI (BA-F8 at 1:25 dilution, igG2b), MHCIIA (SC-71 at 1:500 dilution, igG1), and MHCIIB (BF-F3 at 1:50 dilution, igM) for 2 hours. Fibres that were not stained were considered MHCIIX fibres. The slides were washed with PBS and incubated with secondary antibodies for 1 hour. An additional 5 minute PBS wash was conducted, and the slides were mounted with ProLong antifade reagent. Slides were imaged using the EVOS imager, and cross-sectional area was analyzed to determine fiber-type specific atrophy within the muscle samples.

4.6 Flow Cytometric Analyses

4.6.1 Tissue Preparation

The gastrocnemius and soleus muscles were individually prepared for flow cytometric analyses. Each muscle was minced into 1-2 mm pieces and placed into an enzymatic solution containing 0.005 g collagenase (Worthington Biochemical) and 0.02g dispase (Sigma) in 10 mL Ham's F10 Media. The tissues were digested for 60 minutes at 37°C and 140 rpm and then triturated and filtered using a 100-micron mesh. Heat shocked fetal bovine serum (FBS) was added to each mix prior to centrifugation and removal of the supernatant. Red blood lysis buffer was also added to each mix and the suspensions were kept on ice until ready for use.

4.6.2 Antibody Preparation and Staining Procedure

FACS buffer (2% heat shocked FBS in phosphate buffered saline (PBS)) was added to each muscle digestion and the cell suspension was transferred to a 96 well plate in duplicates. Cells were washed in FACS buffer and resuspended in diluted (1:100) normal rat serum in FACS

buffer (Fc block) and incubated on ice for 10 minutes to prevent non-specific antibody binding. Cells were then washed again and resuspended in 50 uL antibody mix prepared as described in Table 1. The cells were incubated in the dark at 4°C for 15 minutes, followed by 37°C for 15 minutes, for a total of 30 minutes of incubation. Then, the cells were washed twice and resuspended with FACS buffer and kept in the dark on ice until ready for use.

4.6.3 Flow Cytometry

The stained cells were analyzed by flow cytometry using the Attune NxT cytometer. The macrophage population was defined as $CD45^{+}CD11b^{+}F4/80^{+}$ cells. Reactive oxygen species (ROS) production and changes in reduced glutathione levels (GSH) were also assessed within the macrophage population. Unstained cells, compensation, and fluorescence minus one (FMO) wells were used as controls to aid in analysis. Rainbow beads (Spherotech Inc) were used prior to each flow cytometry experiment for calibration. The isolated cells were analyzed using the FlowJo software.

4.7 Quantitative Real Time Polymerase Chain Reaction (RT-qPCR)

Extensor digitorum longus (EDL) samples were used for RT-qPCR due to tissue limitations. This muscle was selected for similarity in myosin heavy chain fiber type expression with the gastrocnemius muscle (type IIB rich). For RNA extraction, samples were lysed using TRIzol reagent (Thermo Scientific) and RNA was separated to an aqueous phase using chloroform. The aqueous layer containing RNA was then mixed with isopropanol and loaded to Aurum Total RNA Mini Kit columns (Bio-Rad). Total RNA was then extracted according to the manufacturer's instructions and concentration was assessed on the Nanodrop One (Thermo Scientific). Reverse transcription of RNA into cDNA was performed by M-MLV reverse

transcriptase and oligo(dT) primers (Qiagen). cDNA was then amplified in a CFX384 Touch Real-Time PCR Detection Systems (Bio-Rad) with a SYBR Green master mix and specific primers, listed below in Table 2. Gene expression was normalized to a Rplp0 control, and relative differences were determined using the ΔΔCq method. Values are presented as fold increases relative to GS control group.

4.8 Statistics

All results were expressed as mean ± SD with the level of statistical significance established at $p < 0.05$ for all statistics. All data was subjected to ROUT test to identify and exclude any outliers (Q=0.05). The D'Agostino-Pearson omnibus normality test was used to determine if data fit a normal Gaussian distribution. If data did not fit a normal distribution, a non-parametric Kruskal-Wallis test was performed. A parametric one-way ANOVA was used for data that conformed to a normal distribution, unless otherwise stated. The Benjamini, Krieger, and Yekutieli post hoc test was used to correct for a false discovery rate (FDR). All reported *p values* are FDR-adjusted *p values* (termed as '*q*'). All statistical analyses were performed with GraphPad Prism Software (Version 9.4.1.458).

Table 1: Antibody Preparation

CD11b	1:100
CD45	1:400
F4/80	1:50
Mitosox	2.5 uM
Monobromobimane (mBBr)	40 uM

Table 2: PCR Primers

Primer	**Sequence**
Lyve1 FWD	CTA TGG ATG GGT TGG AGA ACA G
Lyve1 REV	TGG AGG GAG CAT TCC AAA TC
Timd4 FWD	GGC CAG ACA ACA CTG AAG ATA G
Timd4 REV	ATG GTG AGT CAG AGA GTG AAG A
FCNA FWD	AGG TCA CCA CTA CTC CTA CAA
FCNA REV	CTT CTA GAG ATC CCT CCC TTC A
Folr2 FWD	CTC CTA CAA GGT CAG CAA CTA C
Folr2 REV	ACT TCA CCA CGT CCT CAT TC

Chapter 5: Results

5.1 Anthropometric data in the modified EAM model

A three phase study was conducted to assess changes in the EAM model over time, as described earlier in Methods (Figure 5A). Muscle wet weights were measured in the tibialis anterior (TA), extensor digitorum longus (EDL), plantaris (PLT), quadriceps (QUAD), gastrocnemius (GAS), and soleus (SOL) muscles. Raw weights did not change significantly between experimental groups for any of the three phases (Figure 5C, F, I). Weights were also recorded in the spleen and significant differences were observed in all three phases. In each phase, both GCI and M groups had significantly higher spleen weights than the GS control groups (Figure 5D, G, J). Phase 2 had the highest change in weight, with a 56.85% increase in weight in the GCI group, and a 44.38% increase in the M group compared to GS (Figure 5G). Phases 1 and 3 had a 33.34%, and 35.87% increase in the GCI group, and a 39.78% and 35.5% increase in the M group, respectively, relative to GS (Figure 5D, J). No significance was recorded between the GCI and M groups for any phase (Figure 5D, G, J). Additional organs collected included the kidney, liver, inguinal white adipose tissue (iWAT), lungs, and heart (Table 3). Kidney weights were significantly higher in GCI and M (compared to GS), in phases 1 and 2, and liver weights were higher in the same groups for phase 1. Additionally, the heart weight was elevated in GCI and M (compared to GS) in phase 1 (Table 3). Body weight measurements were also collected and recorded as a percentage (%) change between the first day of injections and the date of sacrifice (Figure 5B, E, H). These measurements were assessed within each phase. Phases 2 and 3 both had significantly higher changes to % body weight in the M group compared to GS (Figure 5E, H). Phase 3 also had a significant increase in the GCI

group weight change compared to GS, but no differences were recorded between GCI and M (Figure 5H).

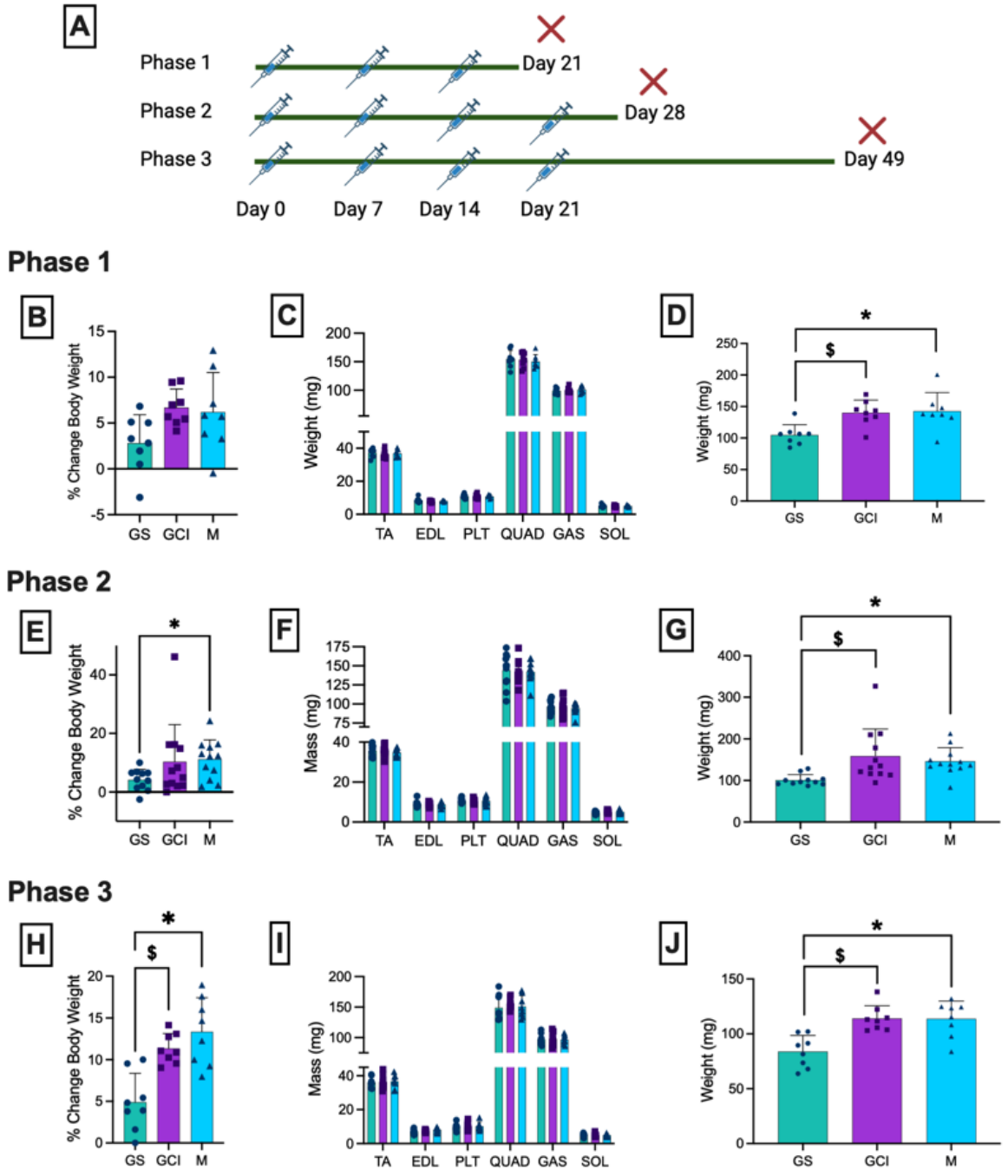

Figure 5: EAM Model Anthropometric Data.

A three phase study design was employed to assess EAM (A). Bodyweight measurements are shown as a % change between the initial injection date (day 0) and the corresponding date of tissue collection for phase 1 (B), phase 2 (E), and phase 3 (H). Muscle weights (mg) were

compared between GS, GCI, and M across all three phases (C,F,I). The tibialis anterior (TA), extensor digitorum longus (EDL), plantaris (PLT), quadriceps (QUAD), gastrocnemius (GAS), and soleus (SOL) muscles were collected and weighed on the date of tissue collection. Spleen weights (mg) are shown across phase 1 (D), phase 2 (G), and phase 3 (J). Results are represented as mean ± SD, n=8-12, *p<0.05 in GS compared with M, #p<0.05 in GCI compared to M, and \$$p$<0.05 in GS compared with GCI.

Table 3: Organ Weights (mg)
Organ weights (mg) were recorded for GS, GCI, M groups within each phase at the time of tissue collection. Results are represented as mean ± SD, n=8-12, *p<0.05 in GS compared with M, #p<0.05 in GCI compared to M, and \$$p$<0.05 in GS compared with GCI.

	Kidney	Liver	Adipose Tissue	Lung	Heart
PHASE 1					
GS	134.8$^{\$*}$	942.9$^{\$*}$	275.5	166.6	112.9$^{\$*}$
GCI	148.8	1111	253.5	187.8	120.5
M	154.0	1086	264.5	199.9	121.6
PHASE 2					
GS	132$^{\$*}$	947.2	247.6	164.2	115.7
GCI	147.2	1058	249.9	189.5	120.4
M	145	1094	260.2	178.7	116.4
PHASE 3					
GS	132.2	853	266.6	168.4	114
GCI	130.9	975.4	281.2	193.7	115.5
M	134.9	1041	276.4	170.1	113.8

5.2 Functional assessments of strength in the modified EAM model

Functional testing was conducted using grip strength and cage hang time measures for all experimental groups. Maximal grip strength values over three trial attempts did not show any significant changes between experimental groups within any phase (Figure 6A-C). Maximal cage hang time in phase 1 showed a 28.55% decrease in the GCI group compared to both GS and M groups and a 38.58% decrease in the same groups of phase 2 (Figure 6D, E). No changes were observed in cage hang time maximum in phase 3 (Figure 6F).

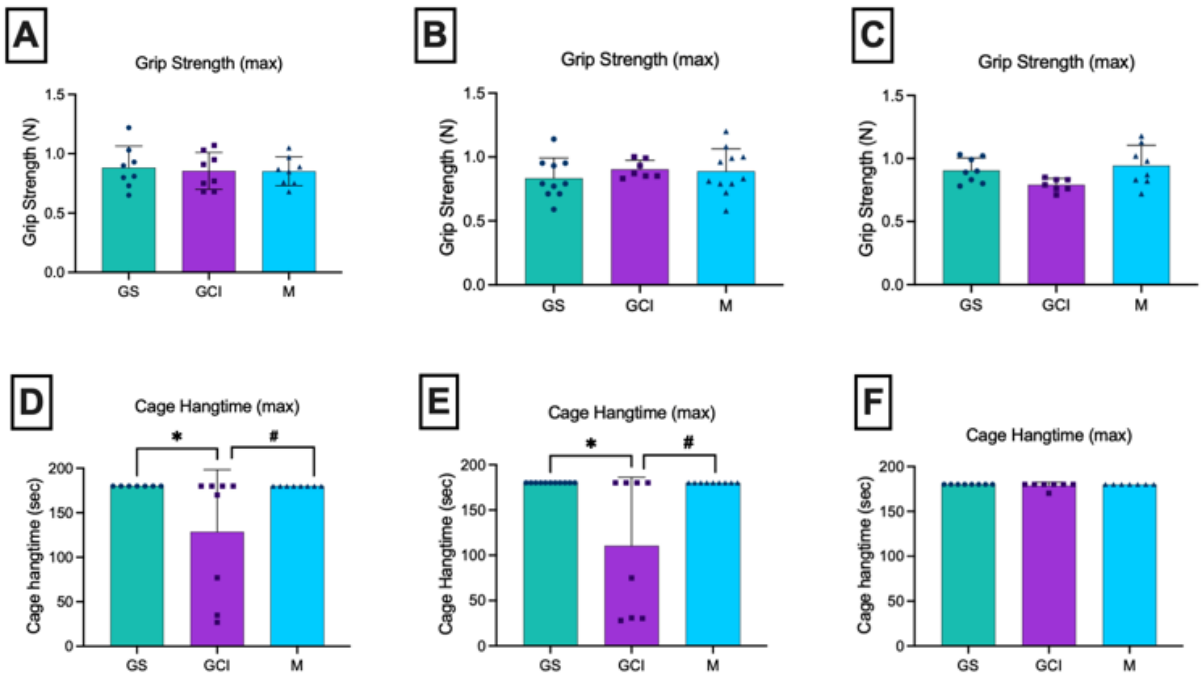

Figure 6: Functional testing through grip strength and cage hang time.
Both grip strength and cage hang time were reported as a maximum value out of three trials. These measurements were conducted on the date of tissue collection. Phase 1 is represented in panels A,D; phase 2 is represented by B,E; phase 3 is shown in C,F. Results are represented as mean ± SD, n=8-12, *p<0.05 in GS compared with M, #p<0.05 in GCI compared to M, and \$$p$<0.05 in GS compared with GCI.

5.3 Lack of fibre specific atrophy (CSA)

Myosin heavy chain (MHC) specific staining was conducted to observe changes in the size of the four muscle fibre types in the gastrocnemius muscle to assess muscle fibre atrophy. Type I fibres are stained blue, type IIa as green, type IIx as black (no stain), and type IIb as red (Figure 7D). Measurements are shown as cross sectional area (μm^2). No changes were observed across experimental groups within each phase (Figure 7).

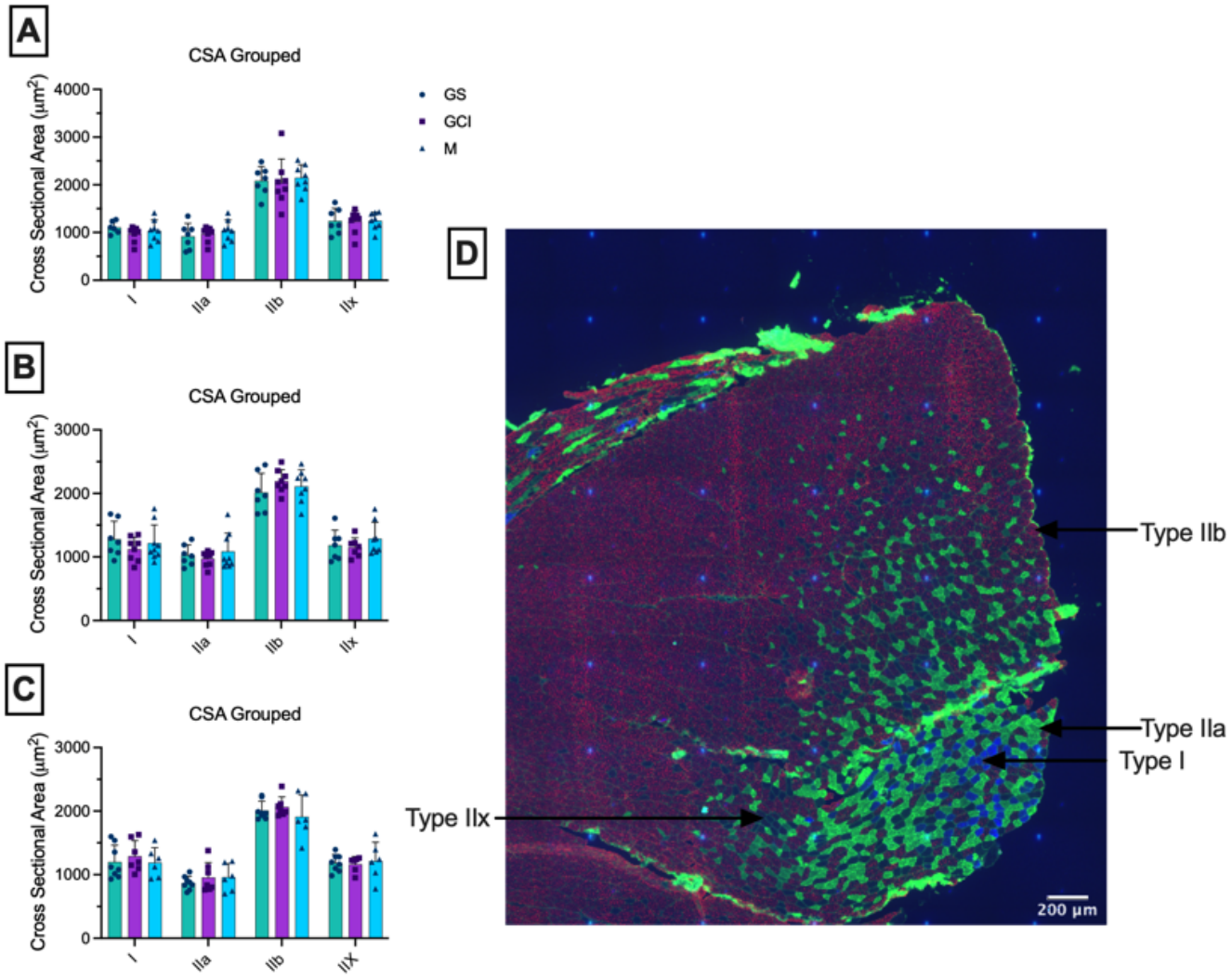

Figure 7: Myosin Heavy Chain (MHC) staining evaluation.
MHC staining of the gastrocnemius muscle was assessed as cross sectional area (CSA) (µm^2). Panels A represents phase 1, panel B shows phase 2, and panel C represents phase 3. Panel D is a section of a sample gastrocnemius MHC stain and fibre types are shown pointing to their respective stain/colour. Results are expressed as mean ± SD, *n*=8-12.

5.4 Histological assessments of inflammation (H&E)

Hematoxylin and eosin staining was used to assess immune cell infiltration in the gastrocnemius and soleus muscles (Figure 8). The gastrocnemius muscle was assessed in all three phases (Figure 8A-C), and the soleus muscle was assessed in phase 3 only (Figure 8D) due

to feasibility. Immune cell infiltration was represented as a percentage (%) of the total muscle cross sectional area. No significant differences were found in the total % of visible immune cell infiltration for either muscle tissue (Figure 8). In phase 2 of the gastrocnemius muscle, the GCI and M groups appeared to have slightly elevated % immune cell infiltration compared to GS, although not significant (Figure 8B).

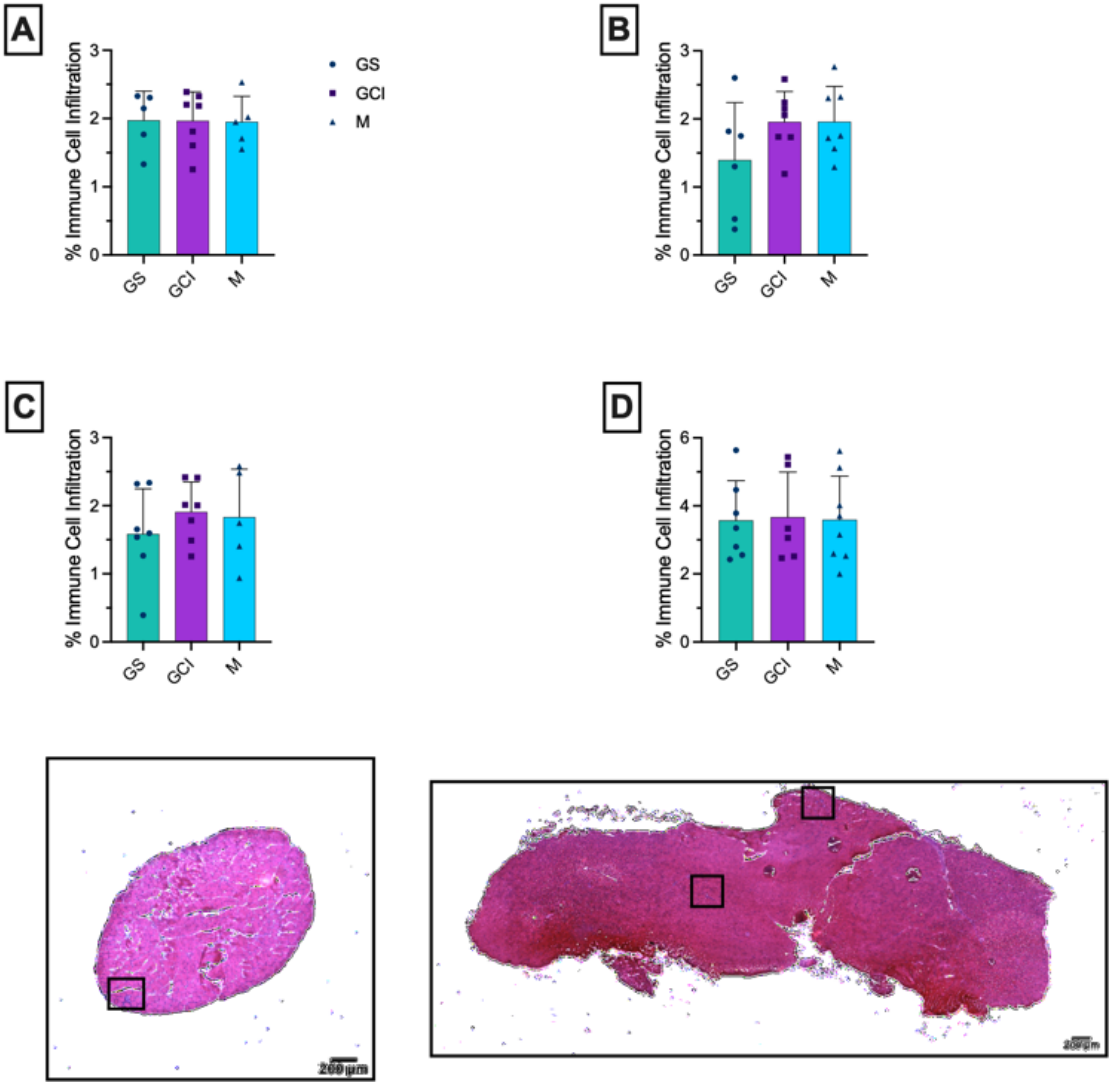

Figure 8: Hematoxylin and eosin (H&E) staining for % immune cell infiltration.
H&E staining was performed on gastrocnemius (GAS) and soleus (SOL) muscles to assess the percentage (%) of immune cell infiltration within muscle cross sections. Sample images of the soleus (left) and gastrocnemius (right) muscles are shown from the M group, with areas of

infiltration highlighted. Assessments were made using ImageJ software. Results are represented as mean ± SD, *n*=8-12.

5.5 The effect of modified EAM induction on lesion development

The presence of subcutaneous lesions at injection sites were assessed daily during monitoring checks for animal wellness and scored according to Table 4. All injection sites were assigned a score, and daily scores were represented as the sum of scores for each mouse. All phases showed higher daily lesion scores in the M group (Figure 9A, B). The GS group exhibited lower lesion scores than the GCI and M groups throughout all three phases. Phase 3 had similar lesion scores for both GCI and M groups, but after day 28, lesion scores spiked in the M group (Figure 9C). Slight increases in the lesion scores were recorded following injection days (day 0, day 7, day 14 for phases 1-3, and day 21 for phases 2-3) (Figure 9).

Table 4: Lesion score grading scale for daily monitoring checks.

Lesion Scale	
No lesions	0
Small bump at injection site	1
Larger bump at injection site	2
Small scab forming at injection site	3
Large scab forming at injection site	4
Continued bleeding (blood on coat, signs of animals picking)	5
Unknown; an odd wound or abnormality around injection areas that was not seen previously	6

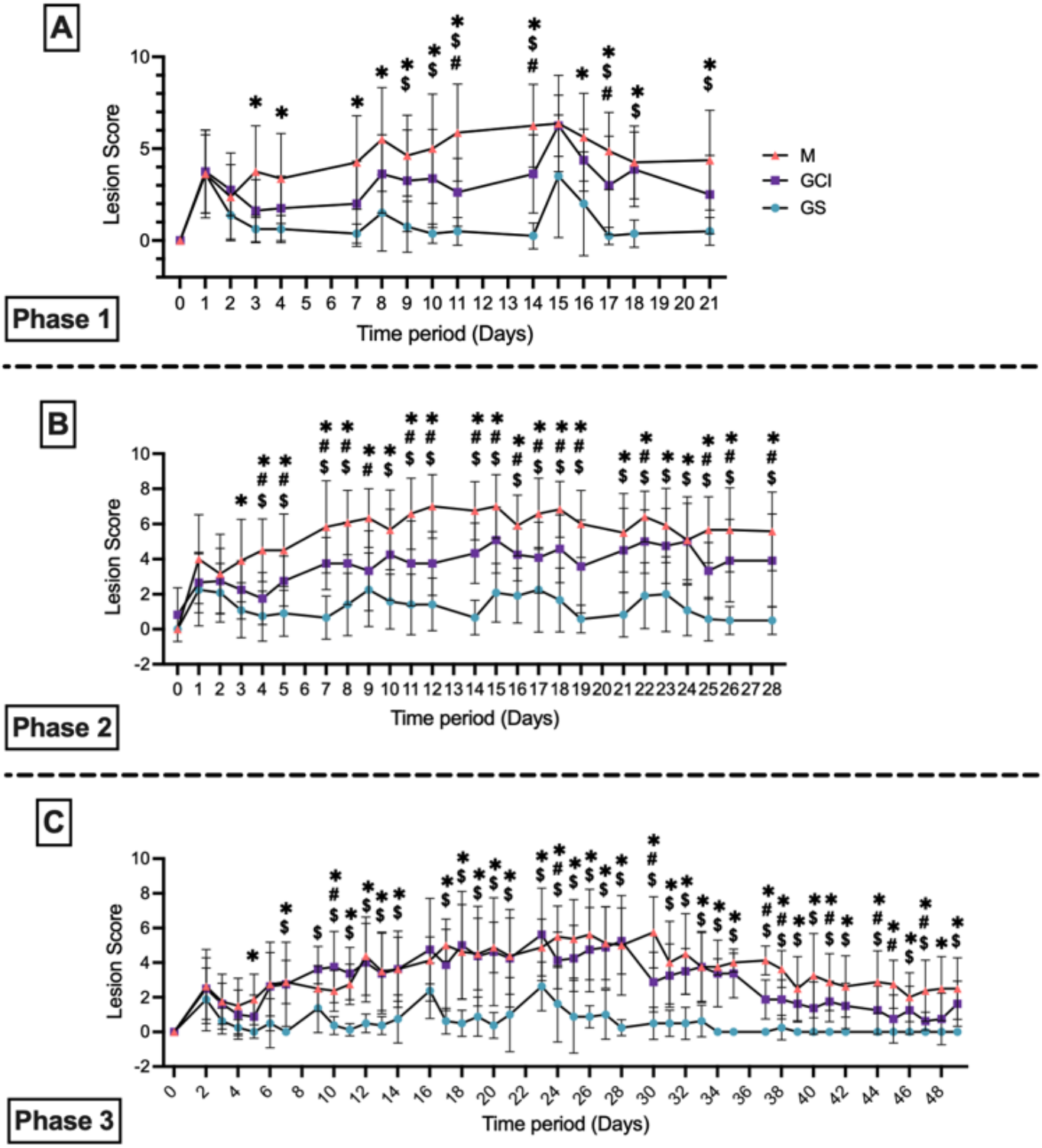

Figure 9: Daily lesion scoring assessment.

Lesions scores were assessed during daily monitoring checks daily for phase 1 (A), phase 2 (B), and phase 3 (C), based on the scoring chart described in Table 2. Results are represented as mean

± SD, n=8-12, *p<0.05 in GS compared with M, #p<0.05 in GCI compared to M, and \$$p$<0.05 in GS compared with GCI.

5.6 Flow cytometric analysis of muscle tissue

The gastrocnemius and soleus muscles were collected and assessed for changes in muscle specific immune responses using flow cytometry. The analysis was conducted using FlowJo Version 9 (Oregon, 2011), and single cells were isolated using two gating strategies shown in Figure 10. Then, cells were filtered according to the expression of CD45 (pan-leukocyte), CD11b (pan-myeloid cell), and F480 (macrophage) markers, in that order (Figure 10). Primarily, the presence of immune cells was assessed as the frequency (%) of macrophages in the single cell population, defined as CD45+ CD11b+ F480+ cells (Figure 11A, D). In the gastrocnemius muscle, there was a significantly higher frequency of macrophages observed in phase 3. Additionally, throughout all three phases for this muscle, the macrophage population was highest in the M group, followed by GCI, and lowest in GS (Figure 11A). Interestingly, in the soleus muscle, the frequency of macrophages remained constant in the GS group across all three phases, while the M and GCI groups fluctuated (Figure 11D). In both the M and GCI groups, there was a slight spike in macrophage frequency in phase 2, which was lowered by phase 3 (Figure 11D).

Macrophage redox characteristics were also assessed in both the gastrocnemius and soleus muscles through the detection of superoxide using mitosox red dye, and reduced glutathione, using monobromobimane (mBBr) dye. First, the percentage of mBBr and mitosox red positive macrophages were assessed in both muscles (Figure 11B-C, E-F). In the gastrocnemius, the GS group had a higher percentage of mBBr positive macrophages in phases 2 and 3, but also had the highest percentage of mitosox red positive macrophages in phase 2 (Figure 11B-C). While the GCI and M groups had similar findings for mitosox red positive macrophages (Figure 11C), GCI

had lower mBBr positive macrophages in phases 2 and 3, and M had the lowest across all three phases (Figure 11B). The detection of reduced glutathione and superoxide in macrophages was also measured as mean fluorescence intensity (MFI) of mBBr and mitosox red, respectively. In the gastrocnemius muscle, no significant differences were observed in either measurement in phases 1 or 2 (Figure 12). However, in phase 3, mBBr MFI was significantly lower in both GCI and M compared to GS (Figure 12C). Additionally, mitosox MFI was elevated in both GCI and M groups (compared with GS) in phase 3 but the change was only significant in GCI (Figure 12F).

In the soleus muscle, the M group showed decreased mBBr positive macrophages, paired with the highest presence of mitosox positive macrophages in phase 3 (Figure 11E-F). Interestingly, mBBr positive macrophages were lower in both GCI and M groups within phase 3 (Figure 11E). Mitosox positive macrophages were both lower in GS and GCI across all three phases (Figure 11F). In terms of mitosox and mBBr expression measured as MFI, there were no significant differences observed within any phase (Figure 13). However, the M group appeared to have lower mBBr MFI as well as a slightly elevated mitosox MFI measurements across all three phases (Figure 13).

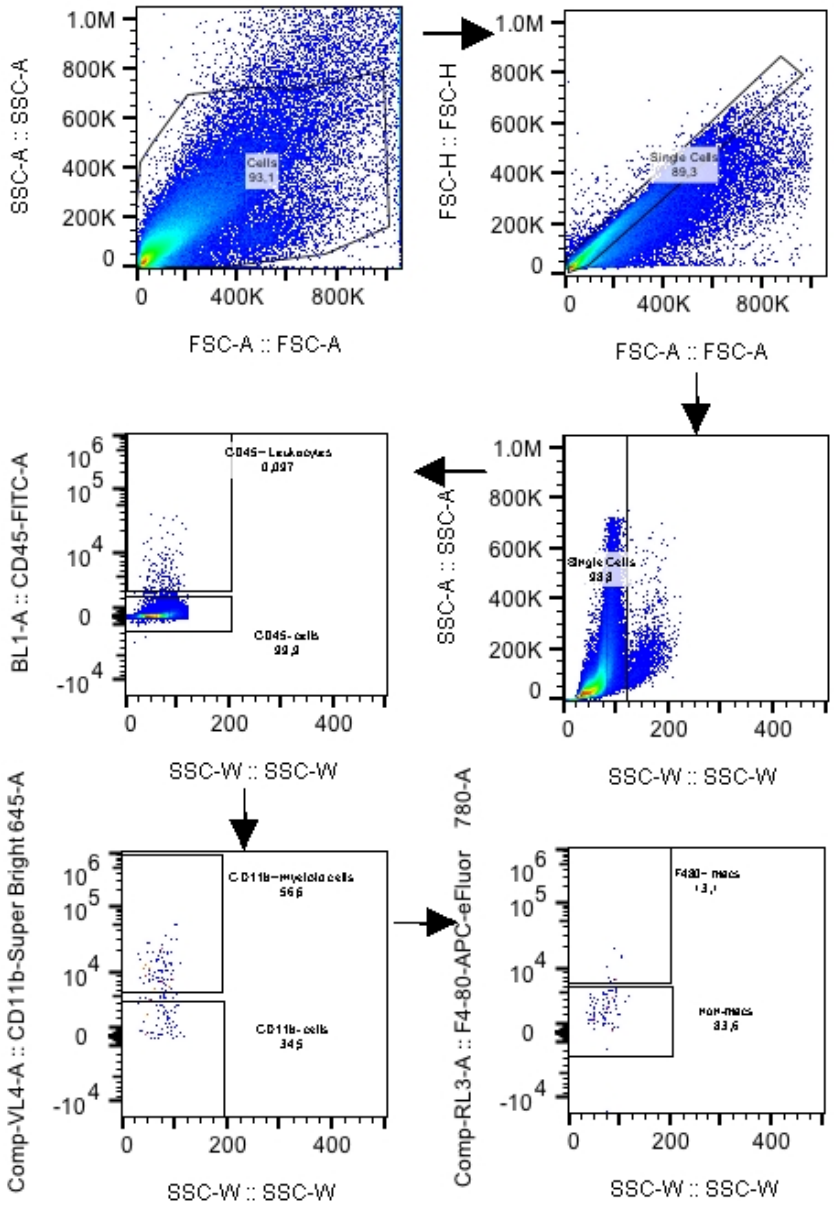

Figure 10: Flow Cytometric Analysis Gating Strategy.

This gating strategy was implemented using FlowJo (Version 9). It was applied to all samples for both the gastrocnemius and soleus muscles. Single cells were filtered twice, and then cells were separated according to the expression of CD45, CD11b, and F480 markers.

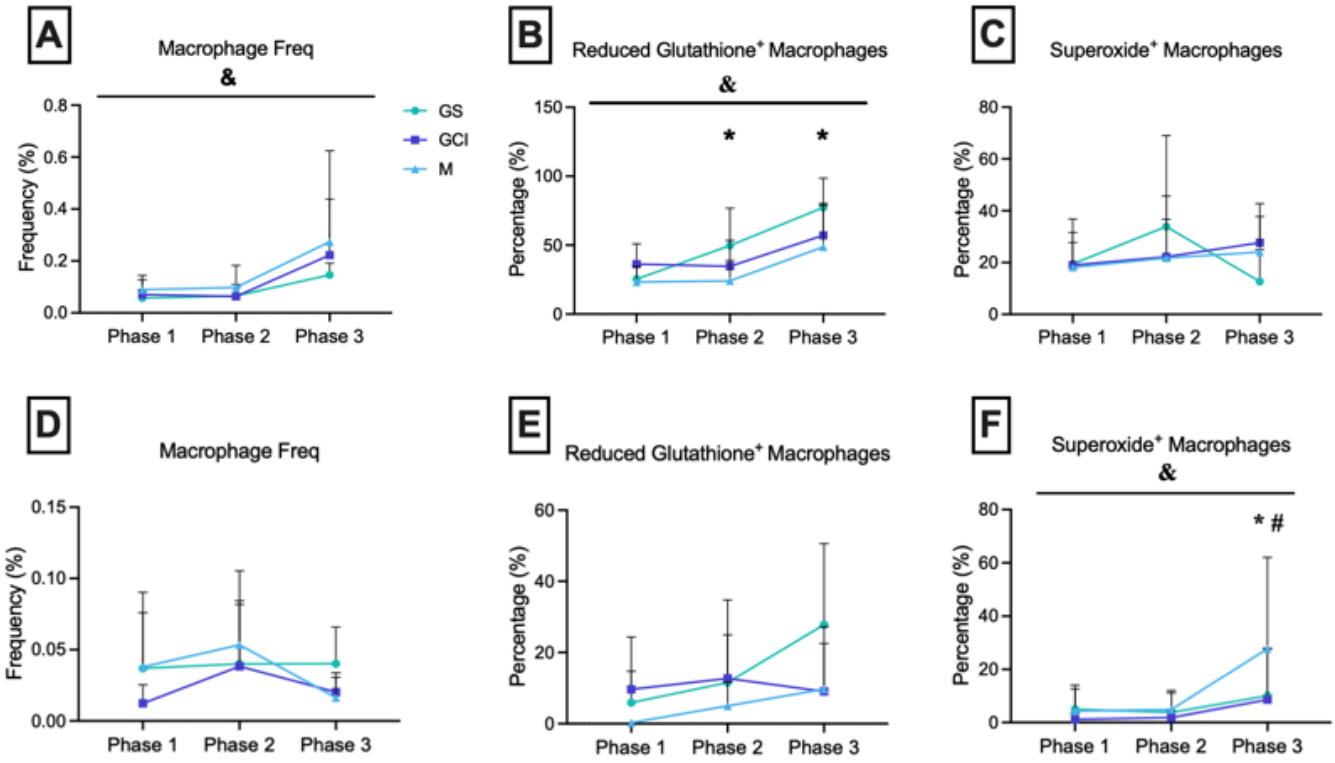

Figure 11: Muscle specific macrophage frequencies and characteristics.

Muscle specific macrophage characteristics are shown in the gastrocnemius (A-C), and soleus (D-F) muscles. Macrophages were defined as CD45+ CD11b+ F480+ cells, and frequencies are shown as a percentage (%) of the single cell population. Detection of reduced glutathione (using monobromobimane (mBBr)) and superoxide (using mitosox) (B-C, E-F) are shown as the percentage of macrophages positively fluorescing. A two-way ANOVA was conducted to compare experimental groups and phases, and results are represented as mean ± SD, n=8-12, *p<0.05 in GS compared with M, #p<0.05 in GCI compared to M, \$$p$<0.05 in GS compared with GCI, and *&<0.05* denotes an effect across phases.

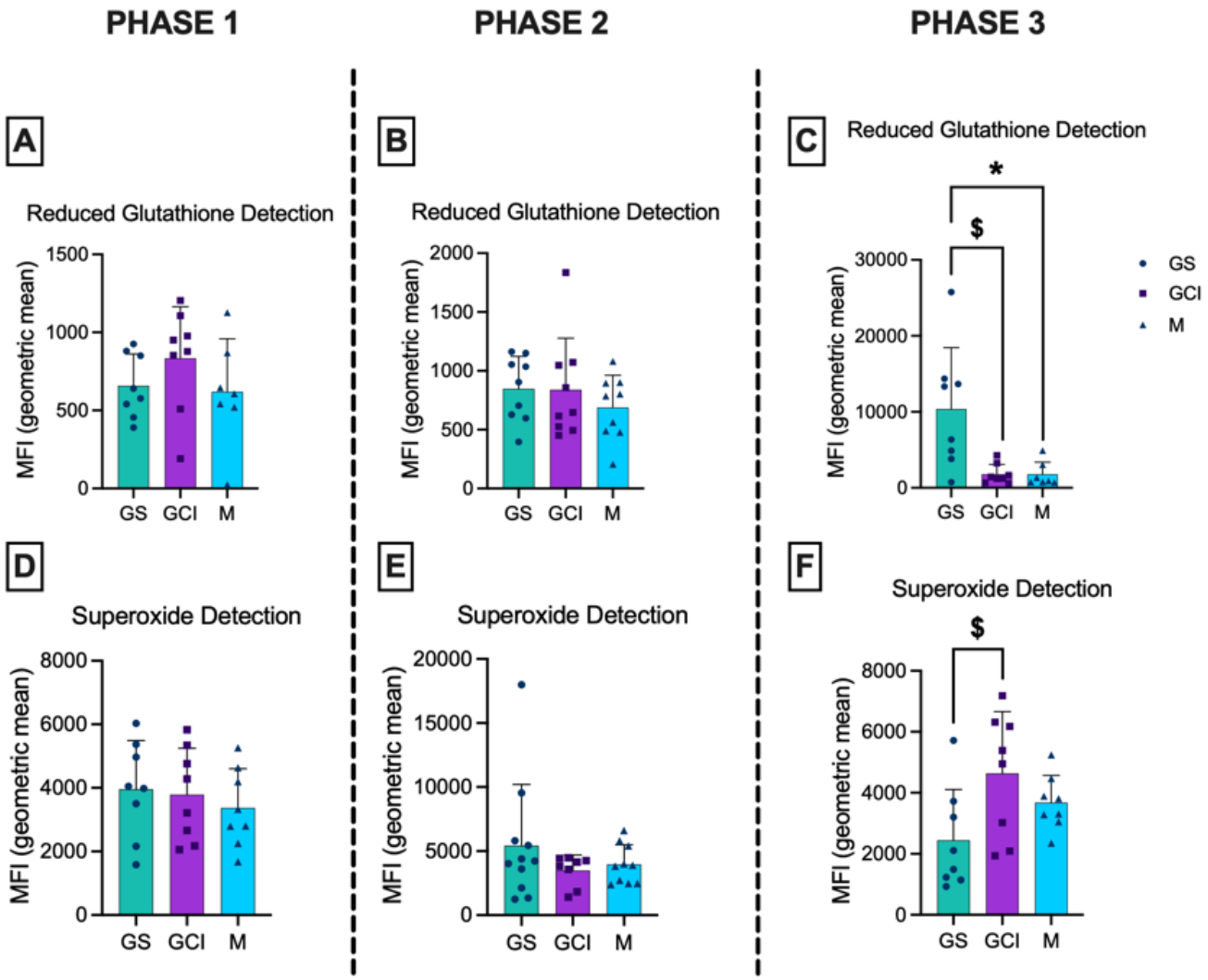

Figure 12: Gastrocnemius specific macrophage reduced glutathione and superoxide detection.

Detection of reduced glutathione (mBBr) and superoxide (mitosox red) are shown as a geometric mean of mean fluorescence intensity (MFI) measured through flow cytometry. Results are shown for phase 1 (A,D), phase 2 (B,E), and phase 3 (C,F). Results are represented as mean ± SD, n=8-12, *p<0.05 in GS compared with M, #p<0.05 in GCI compared to M, and \$$p$<0.05 in GS compared with GCI.

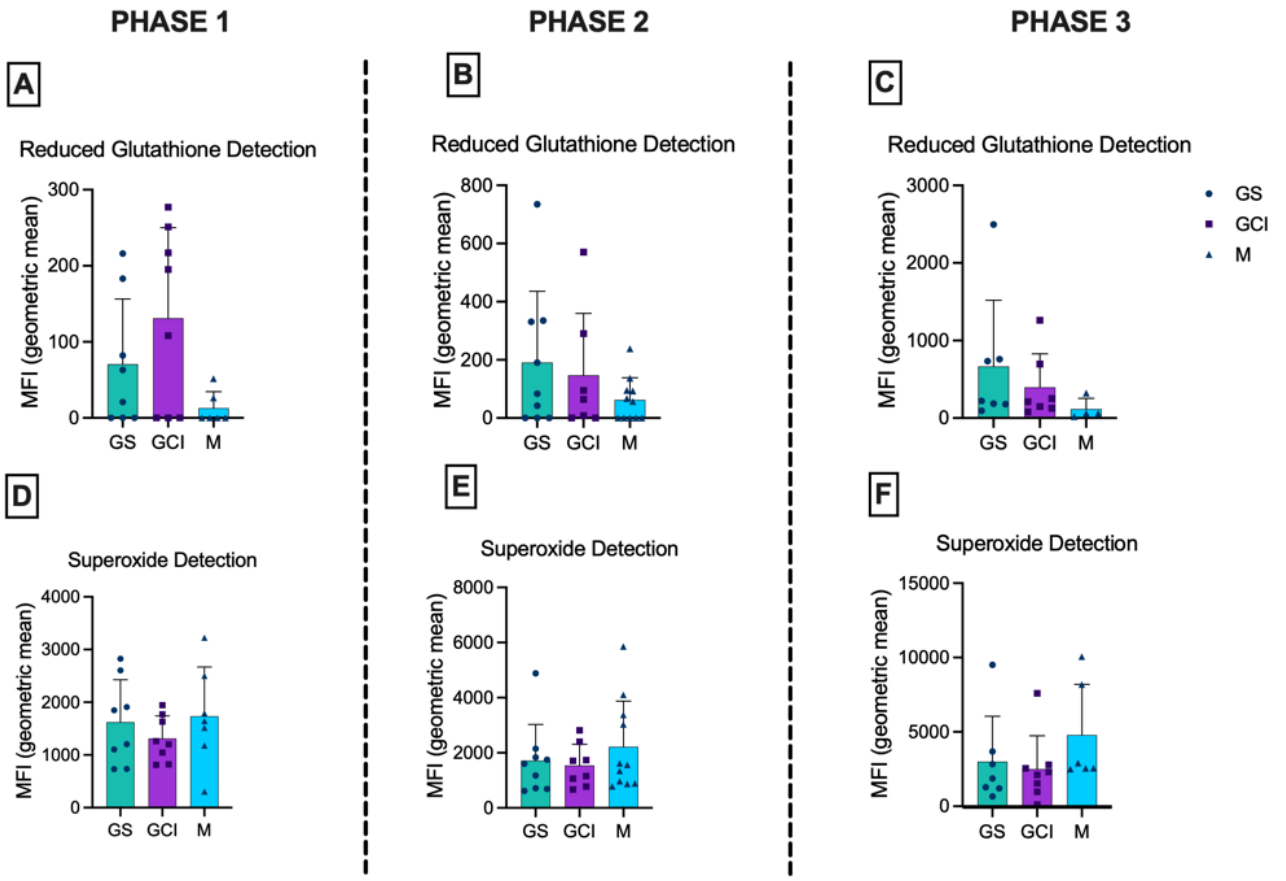

Figure 13: Soleus specific macrophage reduced glutathione and superoxide detection.

Detection of reduced glutathione (mBBr) and superoxide (mitosox red) are shown as a geometric mean of mean fluorescence intensity (MFI) measured through flow cytometry in the soleus muscle. Results are shown for phase 1 (A,D), phase 2 (B,E), and phase 3 (C,F). Results are represented as mean ± SD, n=8-12, *p<0.05 in GS compared with M, #p<0.05 in GCI compared to M, and $$p$<0.05 in GS compared with GCI.

5.7 Real Time quantitative Polymerase Chain Reaction (RT-qPCR) analysis of EAM muscle tissue

RT-qPCR was used to assess the expression of various markers in the extensor digitorum longus (EDL) muscle. First, the expression of peroxiredoxin-5 (PRDX5), an antioxidant, was measured for each phase as a fold change in mRNA, using RPLP0 as a housekeeping gene. No significant differences were observed in phases 1 and 2 (Figure 14A-B). However, in phase 3,

both GCI and M groups had significantly higher expression of PRDX5 compared to GS. There were no differences observed between GCI and M (Figure 14C).

Next, IL-6 and IL-1β cytokines, s100a8, and s100a9 mRNA expression were measured to assess a pro-inflammatory related response. Additionally, Lyve1, TIMD4, FCNA, and Folr2 were measured to assess additional changes to anti-inflammatory responses in this model. Changes in levels of these genes have been reported in macrophages shifting toward a pro or anti-inflammatory response[34]. Results are shown as a fold change in mRNA and expression levels were compared across experimental groups and phases. As part of the pro-inflammatory related genes, IL-6 was elevated in phases 1 and 3, while s100a8 expression increased in phase 3 (GCI>M>GS) (Figure 15). In terms of the anti-inflammatory related genes, an overall phase effect was observed in TIMD4, FCNA, and Lyve1. The expression of these genes was higher in phases 1 and 3. Additionally, there was a significant decrease in expression of Lyve1 in both the M and GCI groups compared to GS (Figure 15).

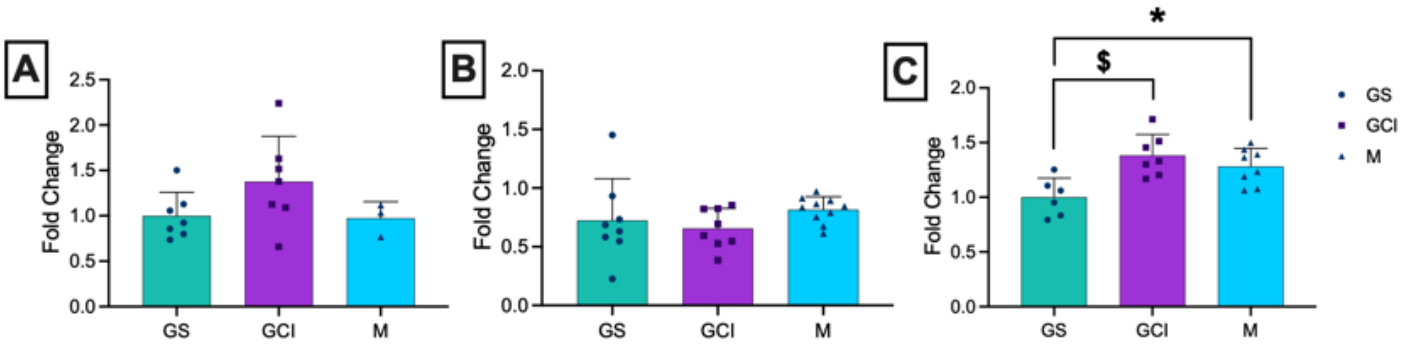

Figure 14: Expression of peroxiredoxin-5 (PRDX5) in EAM.

Changes to PRDX5 mRNA was assessed in the extensor digitorum longus (EDL) muscle for phase 1 (A), phase 2 (B), and phase 3 (C) using RT-qPCR. Results are represented as mean ± SD, n=8-12, *p<0.05 in GS compared with M, #p<0.05 in GCI compared to M, and \$$p$<0.05 in GS compared with GCI.

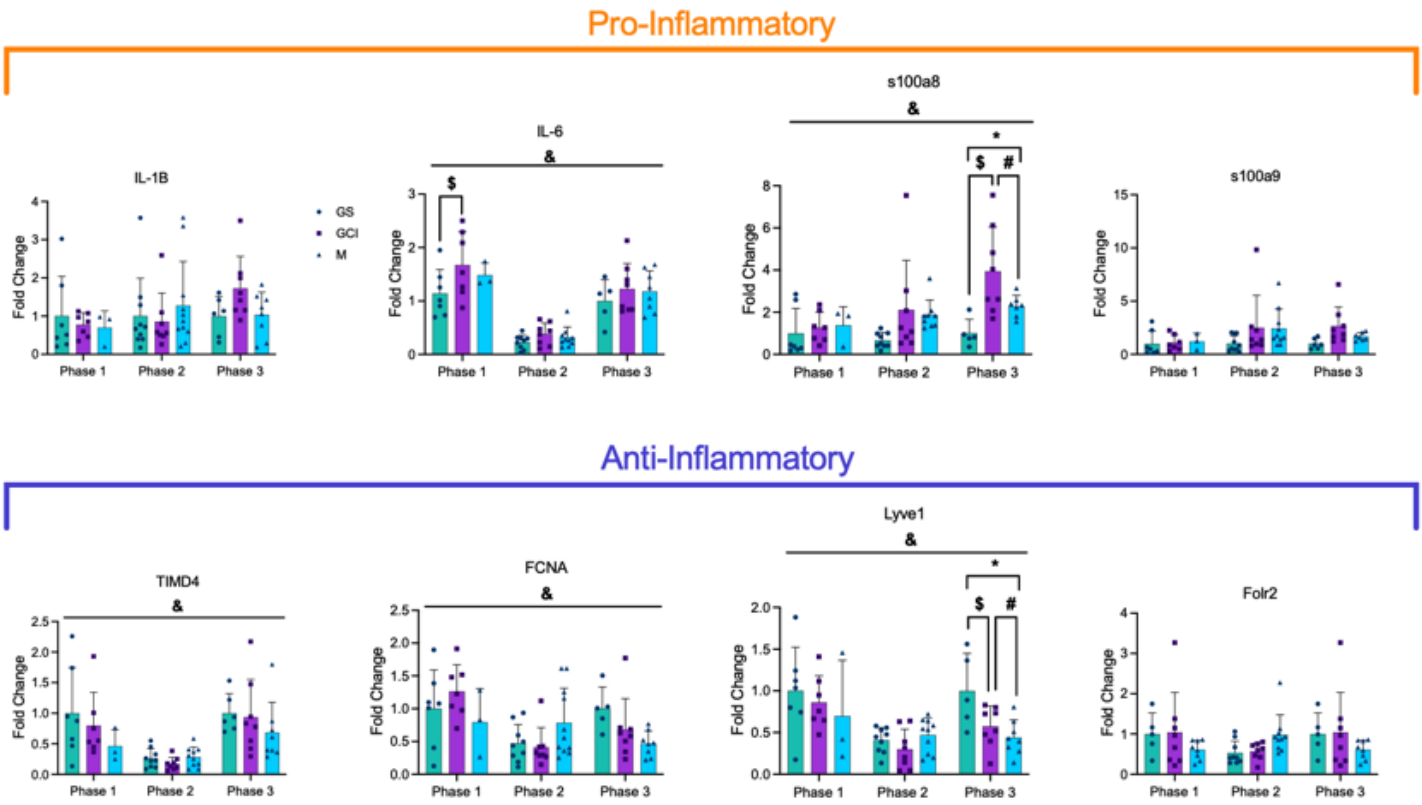

Figure 15: Assessing changes to IL-1B, IL-6, S100a8, s100a9, Lyve1, TIMD4, FCNA, and Folr2 mRNA transcripts.

mRNA levels were evaluated using RT-qPCR in the extensor digitorum longus (EDL) muscle A two-way ANOVA was conducted to compare experimental groups and phases, and results are represented as mean ± SD, n=8-12, *p<0.05 in GS compared with M, #p<0.05 in GCI compared to M, $$p$<0.05 in GS compared with GCI, and *&<0.05* denotes an effect across phases.

Chapter 6: Discussion

6.1 PT-Free Modified EAM Induction

The modified EAM model employed in this thesis was used to assess possible responses to rabbit myosin in a wildtype mouse species in the absence of strong adjuvants and toxins. As previously mentioned in Methods, CFA was added to the primary immunization while IFA was used for all remaining inoculations. Additionally, pertussis toxin was avoided to prevent severe, systemic inflammation and to maintain animal health and wellbeing. The induction of EAM has been well documented in previous models that utilized pertussis toxin (PT) or the SJL/J strain of mice[17, 18, 59]. EAM induction has been characterized as changes in immune cell infiltration at the muscle level, muscle weakness and/or atrophy. Previous research conducted by Himori et al. (2021) showed a 30% decrease in the weight of the gastrocnemius muscle in the EAM treated group[60]. This group induced EAM in female BALB/c mice, using a total of three weekly immunizations of purified rat myosin and CFA, with the use of the pertussis toxin. In our study, the primary assessments conducted included whole body measures of muscle strength (grip strength and cage hang time), muscle wet weights, organ weights, and % changes in body weight. In our modified EAM model, no significant differences were found in the muscle wet weights across any phase (Results- Figure 5). This leads us to believe that introduction of a foreign myosin protein (in our case, rabbit) with a weaker adjuvant is not sufficient to replicate the response observed by other researchers. However, this also leads us to question the impact of using PT in conjunction with CFA on other organ tissues. While research conducted by Allenbach et al. (2009) using the typical EAM model showed no histological abnormalities in the spleen, lungs, small intestine and heart[17], EAM mouse death during a study conducted by Kang et al. (2015) was believed to be due to toxin-induced systemic inflammation using CFA and

PT[19]. This is indicative of the strength of this toxin and emphasizes the importance of developing a model that portrays the human condition, which develops without the involvement of PT. Additionally, in our study, we found spleen weights to be significantly higher in both the GCI and M groups (compared to GS) (Results- Figure 5D, G, J). Enlarged spleens are indicative of an immune response. We observed similar changes in our GCI and M groups, suggesting that an adjuvant-related reaction had occurred, as opposed to a modified-EAM-specific response. Without the use of continuous CFA and PT, we did not observe a different response with the addition of myosin. We also measured weight changes in the kidney, liver, adipose tissue (inguinal white adipose-iWAT), lungs, and heart and observed larger weights in both GCI and M in the kidney (phase 1 and 2), and liver (phase 1) (Results-Table 3). Additionally, an increase in heart weight was observed in GCI and M (compared to GS) in phase 1, albeit this difference was approximately 8 mg, and may be due to variation. In phase 3, no significant differences in organ weights were observed. Additionally, we noticed significantly higher % changes in body weight in our GCI and M groups in phase 3 (Results-Figure 15). It is possible that this increase in size as well as % change in body weight is an adjuvant effect due to inflammation or due to the addition of paraffin oil in both CFA and IFA. However, we did not report any changes in iWAT weight, and the mechanisms of these alterations require further research to be fully understood.

In the EAM model induced by Meyer et al. (2017), grip strength in mice was reported to be 30% lower following EAM induction, again using CFA and PT[59]. In our study, we found no differences in grip strength across any of the three phases but reported decreased cage hangtime maximum in the GCI group in phases 1 and 2. In phase 3, cage hang time was the same across all three groups, and no adjuvant or myosin related differences were observed (Results-Figure 6). Grip strength provides a measure of functional muscle strength, while cage hang time can

provide a measure of fatigue or endurance. Since we only observed changes in our cage hang time measure, it is possible that an adjuvant effect is leading to alterations in muscle fatigue, as opposed to force. However, as this difference was of approximately 60 seconds, it is also possible that it was due to variation in mice. Grip strength and cage hangtime are both voluntary measures of strength and may change depending on the level of compliance.

Additionally, Kang et al. (2015) reported muscle atrophy in the PT-dependent EAM model, although it is not known whether this was specific to one of the four myosin heavy chain (MHC) isoforms[19]. Thus, we assessed atrophy as a measure of cross-sectional area in the gastrocnemius muscle. Using the MHC stain in the Type IIb-rich muscle, we found that the average cross sectional area did not differ significantly for any myosin fibre type (Results- Figure 7). The use of foreign myosin as an antigen did not reproduce the results observed in the traditional EAM model. Using strong toxins such as PT may be resulting in atrophy of muscle fibres through the increased damage and inflammation following immune system overactivation. Our modified model did not target myosin in muscle fibres as robustly as in other studies.

However, we did notice the presence of skin lesions at injection sites over the course of treatment, which were reported as daily scores according to the severity of the lesion. The myosin-treated M group showed more severe lesions than both the GCI and GS control groups in phases 1 and 2. In phase 3, the GCI and M groups had similar severity of lesions throughout the course. Generally, the severity of the scores can be ordered decreasingly as M>GCI>GS (Results-Figure 9). The lesion scores are indicative of an immune response occurring, with more significant changes observed in the M group. As such, we explored the potential immune responses in more detail.

6.2 Immune Cell Infiltration and Characteristics

We used H&E staining to assess the degree of visible immune cell infiltration around muscle fibres in the gastrocnemius (generally MHC type IIb rich) and soleus (MHC type I rich), which is a hallmark feature following EAM induction[17, 18, 59]. While large amounts of visible immune cell infiltrates were observed in these other traditional EAM models, we did not observe similar changes. There were no significant differences between experimental groups reported for any phase of the gastrocnemius. Due to feasibility, we only assessed phase 3 of the soleus muscle, but again, no differences were found (Results-Figure 8). The combination of CFA and IFA in the absence of PT was not strong enough to stimulate movement and infiltration of immune cells into the muscle fibres. The resident immune cells we observed in our H&E staining were similar across all groups. Therefore, we relied on flow cytometry for a more detailed assessment on possible changes to these resident immune cell populations.

First, we assessed the frequency of cells that were identified as macrophages (CD45+ CD11b+ F4/80+) in the gastrocnemius and soleus muscles. In the gastrocnemius muscle, we found increases in the frequency of macrophages in phase 3, compared to phases 1 and 2 for all experimental groups. This suggests there was no change in myosin-induced macrophage infiltration. In the soleus, we found increasing macrophage frequency in phase 2 for GCI and M, indicating an adjuvant effect, although these results were not significant (Figure 11). We also assessed reduced glutathione and mitochondrial superoxide production in the muscle derived macrophages. In the soleus, no significant differences were detected, although across all phases, myosin had decreased reduced glutathione MFI, paired with slightly elevated superoxide MFI (Figure 13). In the gastrocnemius muscle, we also found significantly lower detection of reduced glutathione in both GCI and M groups (compared to GS), which was paired with a significantly

higher detection of superoxide in GCI (compared to GS) in phase 3. Superoxide was elevated in M as well in phase 3, but the result was not significant (Figure 12). The increased mitochondrial superoxide may be associated with the decrease in reduced glutathione. Mitochondrial superoxide is dismutated into H_2O_2, which can exit the mitochondria to be converted into H_2O using cytosolic glutathione. While levels of oxidized glutathione were not assessed in this thesis, it is a known fact that reduced glutathione can be oxidized by glutathione peroxidase in the process of neutralizing H_2O_2[43]. As described in the literature review, part of the macrophage response following activation includes increased production of ROS to aid in mediating pro-inflammatory responses. It is also possible that the reduced glutathione was used to neutralize ROS produced by NADPH oxidases, which were not assessed in this thesis. NADPH oxidases play a crucial role in shifting towards an oxidative environment during an inflammatory response.

Based on this data, it is clear the adjuvant is employing an immune response, although it seems to be a delayed response as differences were not observed in phases 1 or 2. Phase 3 was characterized by a four week wait following the final injection before tissue collection. In previous research done by Meyer et al. (2017) and Allenbach et al. (2009), three sets of weekly injections were used to stimulate PT-induced EAM and tissues were collected two weeks following the final injection[17, 59]. However, in the PT free EAM model described by Suzuki et al. (2005), three sets of immunizations were conducted prior to sacrifice one week after the final injection[18]. It is important to note that Suzuki et al. (2005) used SJL/J mice, which again, are prone to developing a spontaneous myopathy, while Meyer et al. (2017) and Allenbach et al. (2009) used wildtype BALB/c mice. Perhaps the one week post final injection sacrifice date employed in phases 1 and 2 was not sufficient in our modified model with wildtype mice in the

development of a muscle specific immune response. With an increased shift towards oxidation observed only in phase 3, the mice may require a long period of time in order for the macrophages at the muscle level to begin responding.

6.3 Alterations to Gene Expression

The extensor digitorum longus (EDL) muscle was used for RT-qPCR analysis of genes reported to be altered during macrophage polarization. While other analyses were conducted on the gastrocnemius and soleus muscles, we could not use the same muscles due to feasibility and tissue limitations. We selected the EDL based on similarities to the gastrocnemius muscle in terms of MHC fibre type as both are rich in type IIb fibres[61]. First, we assessed the expression of *PRDX5*, a cellular detoxification related gene. Similar to glutathione peroxidases, peroxiredoxins function in maintaining cellular H_2O_2 levels, and serve an antioxidant purpose[62]. Peroxiredoxin-5 is present in both cytosolic and mitochondrial compartments in mammalian cells[63]. The expression of *PRDX5* has been shown to increase in macrophages during an inflammatory response, which may provide a protective mechanism against higher levels of oxidative stress[64]. However, *PRDX5* is also expressed in muscle cells[65], and we conducted RT-qPCR on a muscle homogenate. As such, it is possible that the *PRDX5* we are detecting is present in higher quantities within the muscle cells themselves instead of within macrophages. Despite this limitation, changes in *PRDX5* expression provide us with more detail about the total redox environment with our modified EAM model. The results did not show significant changes in phases 1 and 2, but in phase 3, expression of *PRDX5* was significantly higher in GCI and M (compared to GS) (Results-Figure 14). In addition to the changes observed in phase 3 through flow cytometry, there seems to be a shift towards oxidation, and cells are compensating by

increasing expression of antioxidants. Again, this delayed response may suggest that without strong adjuvants and toxins, a longer time-period may be required for cells at the muscle level to respond. Additionally, we are only observing an effect in groups treated with our adjuvants, suggesting that our myosin is not resulting in enhanced immune cell responses.

We also assessed the expression of *IL-1β*, *IL-6*, *s100a8*, *s100a9*, *TIMD4*, *FCNA*, *Lyve1*, and *Folr2* based on research conducted by Krasniewski et al. (2022), which employed single cell RNA-sequencing to identify changes in gene expression within macrophage subpopulations[34]. As discussed previously, macrophage polarization can lead to a wide spectrum of responses, one extreme of which may be associated with the expression of *TIMD4, FCNA, Lyve1, and Folr2* in M2-like polarized macrophages, and may be associated with an anti-inflammatory response. In contrast, the expression of *IL-1β*, *IL-6, s100a8*, and *s100a9* are upregulated with pro-inflammatory responses, as these markers are associated with generating inflammation[34]. In the pro-inflammatory genes, expression of *IL-6* was significantly higher in phases 1 and 3, with elevated expression in GCI and M groups (compared to GS). Additionally, *s100a8* expression was higher in phase 3, with GCI showing the highest fold change. Again, an adjuvant effect was observed. With the anti-inflammatory associated genes, a phase effect was observed in the levels of *TIMD4, FCNA,* and *Lyve 1*. In phase 3, expression of these genes was lower in the GCI and M groups, suggesting there may be more of a pro-inflammatory shift stimulated by the use of the adjuvant. Additionally, expression of *Lyve1* was highest in GS, and lower in GCI and M (Results-Figure 15). With an increase in the expression of two pro-inflammatory related genes, and a decrease in expression of one anti-inflammatory gene in our adjuvant treated groups, this modified model may be more characteristic of an adjuvant model, as no myosin specific

phenotype was observed. We are also noticing a change in phase 3, which again, may be suggesting that this model requires time for a response to be observed.

These results allow us to question the effectiveness of using PT as well as CFA in models of myositis. Since the mechanism(s) leading to myositis are still unknown, the traditional models using PT or SJL/J mice are only effective in replicating the phenotype observed with myositis. However, these models do not allow us to study the mechanisms that can lead to myositis as they require the use of strong adjuvants, the absence of which does not result in any myosin-related differences. It is also unknown whether the mechanism of action of these toxins are similar in the etiology of myositis. Additionally, this model requires the use of successive immunizations, which is stimulating excessive inflammation in the mice. In our modified model, we avoided the use of these toxins but used a foreign myosin protein as well as multiple immunizations. However, we still failed to notice a change in our myosin treated groups, and an adjuvant effect was the main finding observed. The use of one CFA injection followed by the weaker IFA still resulted in more immune system alterations than with the addition of myosin. It is crucial to develop a model that can encapsulate the mechanisms leading to this disease, as opposed to stimulating excessive inflammation that may not be specific to myosin.

Chapter 7: Conclusion and Future Directions

7.1 Conclusion

The purpose of this study was to assess a modified model of experimental autoimmune myositis and observe changes over time. We obtained results that varied from those observed in the current literature utilising the traditional model of EAM. While high degrees of immune cell infiltration, muscle weakness and atrophy have been reported in the EAM model, we did not replicate these findings. The lack of pertussis toxin in our study led to varied results, characterized by an attenuated immune response. We also reported similar changes in our adjuvant control group (GCI) and our myosin treated group (M), suggesting that an adjuvant effect was observed. It is important to question the reliability of using the traditional model, which may be creating excessive inflammation through the continued use of strong adjuvants (CFA) and toxins (PT).

Additionally, we originally hypothesized that the EAM phenotype would be transient, and thus employed the use of phase 3, characterized by a longer time frame between the final injection and date of tissue collection. However, we found that phase 3 showed increased levels of oxidation as well as an overall immune cell response, suggesting this model may require time before any immune related changes at the muscle level can occur. The majority of the findings for phases 1 and 2 did not show significant differences, suggesting that tissue collection 7 days after the final injection may not be long enough to induce an immune response in the wildtype strain. Ultimately, a more effective model that encapsulates the human condition more effectively is required to accurately study this disease.

7.2 Future Directions and Limitations

An important future direction for this research is to conduct the assessment of the presence of myositis-specific autoantibodies to determine whether the model accurately portrays a myositis phenotype. Assessing this can guide modifications to the current models and determine whether this phenotype is general muscle inflammation, or myositis specific. The development of an effective model is crucial in the progress of myositis research.

This thesis did have some limitations that may have impacted the strength of this modified model. Primarily, while we compared our modified EAM model to that of a PT-induced model and EAM models using SJL/J mice, we did not use a different strain of mice or a PT + CFA only control group. As such, we relied on previous literature to compare the efficacies of these models. In our project, we used CFA and IFA, the former of which is a weaker adjuvant. We were unable to use CFA for all injections to conserve animal health and wellbeing. Additionally, we were unable to use intracellular markers to further assess macrophage polarization using flow cytometry due to limitations with our ROS measurements. Moving forward, it would also be beneficial to use more timepoints to capture the immune response as the model progresses. Ultimately, despite these limitations, we were guided by the existing literature and created a ‘blended’ version of existing EAM models.

Chapter 8: References

1. Furst DE, Amato AA, Iorga SR, Gajria K, Fernandes AW. 2012. Epidemiology of adult idiopathic inflammatory myopathies in a U.S. managed care plan. *Journal of Muscle and Nerve*. 45(5): 676-683.

2. Lundberg IE, Visser M, Werth VP. 2018. Classification of myositis. *Nature Reviews Rheumatology*. 14(5): 269-278.

3. West AP, Brodsky IE, Rahner C, Woo DK, Erdjument-Bromage H, Tempst P, Walsh MC, Choi Y, Shadel GS, Ghosh S. 2011. TLR signaling augments macrophage bactericidal activity through mitochondrial ROS. *Nature*. 472(7344): 476-480.

4. Rosenberg NL, Ringel SP, Kotzin BL. 1986. Experimental autoimmune myositis in SJL/J mice. *Journal of Clinical and Experimental Immunology*. 68: 117-129.

5. Yadav Rajwahrdhan, Bhowmick S, Gorecki P, O'Rourke J, Cone RE. (2010). Paradoxical effect of pertussis toxin on the delayed hypersentivity response to autoantigens in mice. *PLoS One*. 5(8): e11983.

6. Rayavarapu S, Van der Meulen JH, Gordish-Dressman H, Hoffman EP, Nagaraju K, Knoblach SM. Characterization of dysferlin deficient SJL/J mice to assess preclinical drug efficacy: fasudil exacerbates muscle disease phenotype. *PLoS One Journal.* 5(9): e12981.

7. Yasier M, Goyal M, Sonthalia S. (2022). Corticosteroid adverse effects. Statpearls Publishing.

8. Oldroyd A, Lilleker J, Chinoy H. (2017). Idiopathic inflammatory myopathies-a guide to subtypes, diagnostic approach and treatment. *Clinical Medicine Journal.* 17(4):322-328.

9. Badrising UA, Maat-Schieman MLC, van Houwelingen JC, van Doorn PA, van Duinen SG, van Engelen BGM, Faber CG, Hoodendijk JE, de Jager AE, Koehler PJ, Visser M, Verschuuren JJGM, Wintzen AR. (2005). Inclusion body myositis: clinical features and clinical course of the disease in 64 patients. *Journal of Neurology*. 252:1448-1454.

10. Naddaf E. (2022). Inclusion body myositis: update on the diagnostic and therapeutic landscape. *Frontiers in Neurology.* 13:1020113.

11. Marvi U, Chung L, Fiorentino DF. (2012). Clinical presentation and evaluation of dermatomyositis. *Indian Journal of Dermatology.* 57(5): 375-381.

12. de Camargo LV, de Carvalho MS, Shinjo SK, de Oliveira ASB, Zanoteli E. (2018). Clinical, histological, and immunohistochemical findings in inclusion body myositis. *Biomed Research International Journal*. 5069042.

13. Hallowell RW, Paik JJ. (2022). Myositis-associated interstitial lung disease: a comprehensive approach to diagnosis and management. *Journal of Clinical and Experimental Rheumatology.* 40(2): 373-383.

14. Satoh M, Tanaka S, Ceribelli A, Calise SJ, Chan EKL. (2017). A comprehensive overview on myositis-specific antibodies: new and old biomarkers in idiopathic inflammatory myopathy. *The Clinical Review in Allergy and Immunology*. 52(1): 1-19.

15. Pinal-Fernandez I, Casal-Dominguez M, Mammen AL. (2018). Immune-mediated necrotizing myopathy. *Current Rheumatology Reports*. 20(4): 21.

16. Konishi R, Ichimura Y, Okiyama N. (2023). Murine models of idiopathic inflammatory myopathy. *Journal of Immunological Medicine.* 46(1): 9-14.

17. Allenbach Y, Solly S, Gregoire S, Dubourg O, Salomon B, Butler-Browne G, Musset L, Herson S, Klatzmann D, Benveniste O. (2009). Role of regulatory T cells in a new mouse model of experimental autoimmune myositis. *The American Journal of Pathology.* 174(3): 989-998.

18. Suzuki F, Nanki T, Imai T, Kikuchi H, Hirohata S, Kohsaka H, Myasaka N. (2005). Inhibition of CX3CL1 (fractalkine) improves experimental autoimmune myositis in SJL/J mice. *The Journal of Immunology.* 175: 6987-6996.

19. Kang J, Zhang HY, Feng GD, Feng DY, Jia HG. (2015). Development of an improved animal model of experimental autoimmune myositis. *International Journal of Clinical and Experimental Pathology.* 8(11): 14457-14464.

20. Sugihara T, Sekine C, Nakae T, Kohyama K, Harigai M, Iwakura Y, Matsumoto Y, Miyasaka N, Kohsaka H. (2007). A new murine model to define the critical pathologic and therapeutic mediators of polymyositis. *Journal of Arthritis and Rheumatism*. 56(4): 1304-1314.

21. Okiyama N, Hasegawa H, Oida T, Hirata S, Yokozeki H, Fujimoto M, Miyasaka N, Kohsaka H. (2015). Experimental myositis inducible with transfer of dendritic cells presenting a skeletal muscle C protein derived CD8 epitope peptide. *International Immunology Journal.* 27(7): 327-332.

22. Janeway CR Jr, Travers P, Walport M, Sclomchik MJ. (2001). Principles of innate and adaptive immunity. In *Immunobiology: the immune system in health and disease.* 5th edition.

23. Navegantes KC, Gomes RS, Pereira PAT, Czaikoski PG, Azevedo CHM, Monteiro MC. (2017). Immune modulation of some autoimmune diseases: the critical role of macrophages and neutrophils in the innate and adaptive immunity. *Journal of Translational Medicine.* 15(1): 36.

24. Marshall JS, Warrington R, Watson W, Kim HL. (2018). An introduction to immunology and immunopathology. *Journal of Allergy, Asthma and Clinical Immunology.* 14(49).

25. Wynn TA, Chawla A, Pollard JW. (2013). Macrophage biology in development, homeostasis and disease. *Nature*. 496: 445-455.

26. Mosser DM, Edwards JP. (2009). Exploring the full spectrum of macrophage activation. *Nature Review Immunology.* 8(12): 958-969.

27. Gordon S, Taylor PR. (2005). Monocyte and macrophage heterogeneity. *Nature Review Immunology*. 5: 953-964.

28. Viola A, Munari F, Sanchez-Rodriguez R, Scolaro T, Castegna A. (2019). The metabolic signature of macrophage responses. *Frontiers in Immunology.* 10: 1462.

29. Ivashkiv LB. (2019). IFNy: signalling, epigenetics and roles in immunity, metabolism, disease and cancer immunotherapy. *Nature Reviews Immunology:* 18(9): 545-558.

30. Gordon S. (2002). Alternative activation of macrophages. *Nature Reviews Immunology.* 3: 23-35.

31. Yunna C, Mengru H, Lei W, Weidong C. (2020). Macrophage M1/M2 polarization. *European Journal of Pharmacology.* 877: 173090.

32. Yao Y, Xu XH, Jin L. (2019). Macrophage polarization in physiological and pathological pregnancy. *Frontiers in Immunology.* 10: 792.

33. Walton RG, Kosmac K, Mula J, Fry CS, Peck BD, Groshong JS, Finlin BS, Zhu B, Kern PA, Peterson CA. (2019). Human skeletal muscle macrophages increase following cycle training and are associated with adaptations that may facilitate growth. *Scientific Reports Journal.* 9: 969.

34. Krasniewski LK, Chakraborty P, Cui CY, Mazan-Mamczarz K, Dunn C, Piao Y, Fan J, Shi C, Wallace T, Nguyen C, Rathbun IA, Munk R, Tsitsipatis D, De S, Sen P, Ferruci L, Gorospe M. (2022). Single-cell analysis of skeletal muscle macrophages reveals age-associated functional subpopulations. *eLife*. 11:e77974.

35. Petrof BJ. (2022). Macrophage plasticity in Duchenne muscular dystrophy: a nexus of pathological remodelling with therapeutic implications. *The Journal of Physiology.* 600(15): 3455- 3464.

36. Rostasy KM, Schmidt J, Bahn E, Pfander T, Piepkorn M, Wilichowski E, Schulz-Schaeffer J. (2008). Distinct inflammatory properties of late-activated macrophages in inflammatory myopathies. *Acta Myologica Journal.* 27(2): 49-53.

37. Bogdan C. (2001). Nitric oxide and the immune response. *Nature Immunology.* 2: 907-916.

38. Fernie AR, Carrari F, Sweetlove LJ. (2004). Respiratory metabolism: glycolysis, the TCA cycle and mitochondrial electron transport. *Current Opinion in Plant Biology.* 7(3): 254-261.

39. Alberts B. (2015). Energy conversion: mitochondria and chloroplasts. In *Molecular Biology of the Cell*. 6th edition.

40. Zhao RZ, Jiang S, Zhang L, Yu ZB. (2019). Mitochondrial electron transport chain, ROS generation and uncoupling (Review). *International Journal of Molecular Medicine*. 44(1): 3-15.

41. Stowe DF, Camara AKS. (2009). Mitochondrial reactive oxygen species production in excitable cells: modulators of mitochondrial and cell function. *Antioxidants and redox signaling*. 11(6): 1373-1414.

42. Ribas V, Garcia-Ruiz C, Fernandez-Checa, J. (2014). Glutathione and mitochondria. *Frontiers in Pharmacology*. 5: 151.

43. Lushcak VI. (2012). Glutathione homeostasis and functions: potential targets for medical interventions. *Journal of Amino Acids*. 2012: 736837.

44. Zitka O, Skalickova S, Gumulec J, Masarik M, Adam V, Hubalek J, Trnkova L, Kruseova J, Eckschalger T, Kizek R. (2012). Redox status expressed as GSH: GSSH ratio as a marker for oxidative stress in paediatric tumour patients. *Oncology Letters.* 4(6): 1247-1253.

45. Kelly B, O'Neill LAJ. (2015). Metabolic reprogramming in macrophages and dendritic cells in innate immunity. *Cell Research*. 25: 771-784.

46. Liberti MV, Locasale JW. (2017). The Warburg effect: how does it benefit cancer cells? *Trends in Biochemical Sciences.* 41(3): 211-218.

47. Freemerman AJ, Johnson AR, Sacks GN, Milner JJ, Kirk EL, Troester MA, Macintyre AN, Goraksha-Hicks P, Rathmell JC, Makowski L. (2014). Metabolic reprogramming of macrophages. *Journal of Biological Chemistry.* 289(11): 7884-7896.

48. Tan HY, Wang N, Li S, Hong M, Wang X, Feng Y. (2016). The reactive oxygen species in macrophage polarization: reflecting its dual role in progression and treatment of human diseases. *Oxidative Medicine and Cellular Longevity.* 2016: 2795090.

49. Liu Y, Xu R, Gu H, Zhang E, Qu J, Cao W, Huang X, Yan H, He J, Cai Z. (2021). Metabolic reprogramming in macrophage responses. *Biomarker Research.* 9:1.

50. Infantino V, Iacobazzi V, Palmieri F, Menga A. (2013). ATP-citrate lyase is essential for macrophage inflammatory response. *Biochemical and Biophysical Research Communications.* 440(1): 105-111.

51. O'Neill LAJ, Artyomov MN. (2019). Itaconate: the poster child of metabolic reprogramming in macrophage function. *Nature Review Immunology.* 19: 273-281.

52. Canton M, Sanchez-Rodriguez R, Spera I, Venegas FC, Favia M, Viola A, Castegna A. (2021). Reactive oxygen species in macrophages: sources and targets. *Frontiers in Immunology.* 12: 734229.

53. Iles KE, Forman HJ. (2002). Macrophage signaling and respiratory burst. *Immunologic Research.* 26(1-3): 95-105.

54. Andreyev AY, Kushnareva YE, Starkova NN, Starkov AA. (2020). Metabolic ROS signaling: to immunity and beyond. *Biochemistry (Moscow).* 85(12): 1650-1667.

55. Martinez-Reyes I, Diebold LP, Kong H, Schieber M, Huang H, Hensley CT, Mehta MM, Wang T, Santos JH, Woychik R, Dufour E, Spelbrink J, Weinberg SE, Zhao Y, DeBerardinis RJ, Chandel NS. (2016). TCA cycle and mitochondrial membrane potential are necessary for diverse biological functions. *Molecular Cell Journal*. 61(2): 199-209.

56. Masoud GN, Li W. (2015). HIF-1a pathway: role, regulation and intervention for cancer therapy. *Acta Pharmaceutica Sinica B.* 5(5): 378-389.

57. Fuhrmann DC, Wittig I, Brune B. (2019). TMEM126B deficiency reduces mitochondrial SDH oxidation by LPS, attenuating HIF-1a stabilization and IL-1B expression. *Redox Biology.* 20: 204-216.

58. Forrester SJ, Kikuchi DS, Hernandes MS, Xu Q, Griendling KK. (2018). Reactive oxygen species in metabolic and inflammatory signaling. *Circulation Research.* 122(6): 877-902.

59. Meyer A, Laverny G, Allenbach Y, Grelet E, Ueberschlag V, Echaniz-Laguna A, Lannes B, Alsaleh G, Charles AL, Singh F, Zoll J, Lonsdorfer E, Maurier F, Boyer O, Gottenberg JE, Nicot AS, Laporte J, Benveniste O, Metzger D, Sibilia J, Geny B. (2017). IFN-B induced reactive oxygen species and mitochondrial damage contribute to muscle impairment and inflammation maintenance in dermatomyositis. *Acta Neuropathologica.* 134: 655-666.

60. Himori K, Ashida Y, Tatebayashi D, Abe M, Saito Y, Chikenji T, Westerblad H, Andersson DC, Yamada T. (2021). Eccentric resistance training ameliorates muscle weakness in a mouse model of idiopathic inflammatory myopathies. *Arthritis and Rheumatology.* 73(5): 848-857.

61. Bloemberg D, Quadrilatero J. (2012). Rapid determination of myosin heavy chain expression in rat, mouse, and human skeletal muscle using multicolor immunofluorescence analysis. *PLoS One.* 7(4): e35273.

62. Rhee SG. (2016). Overview on Peroxiredoxin. *Molecules and Cells.* 39(1): 1-5.

63. Seo MS, Kang SW, Kim K, Baines IC, Lee TH, Rhee SG. (2000). Identification of a new type of mammalian peroxiredoxin that forms an intramolecular disulfide as a reaction intermediate. *Journal of Biological Chemistry.* 275(7): 20346- 20354.

64. Abbas K, Breton J, Picot CR, Quesniaux V, Bouton C, Drapier JC. (2009). Signaling events leading to peroxiredoxin 5 up-regulation in immunostimulated macrophages. *Free Radical Biology and Medicine.* 47: 794-802.

65. Kozakowska M, Pietraszek-Gremplewicz K, Jozkowicz A, Dulak J. (2015). The role of oxidative stress in skeletal muscle injury and regernation: focus on antioxidant enzymes. *Journal of Muscle Research and Cell Motility.* 36: 377-393.

66. Scanlon K, Skerry C, Carbonetti N. (2019). Role of major toxin virulence factors in pertussis infection and disease pathogenesis. *Advances in Experiental Medicine and Biology*. 1183: 35-51.

Supplemental Figures

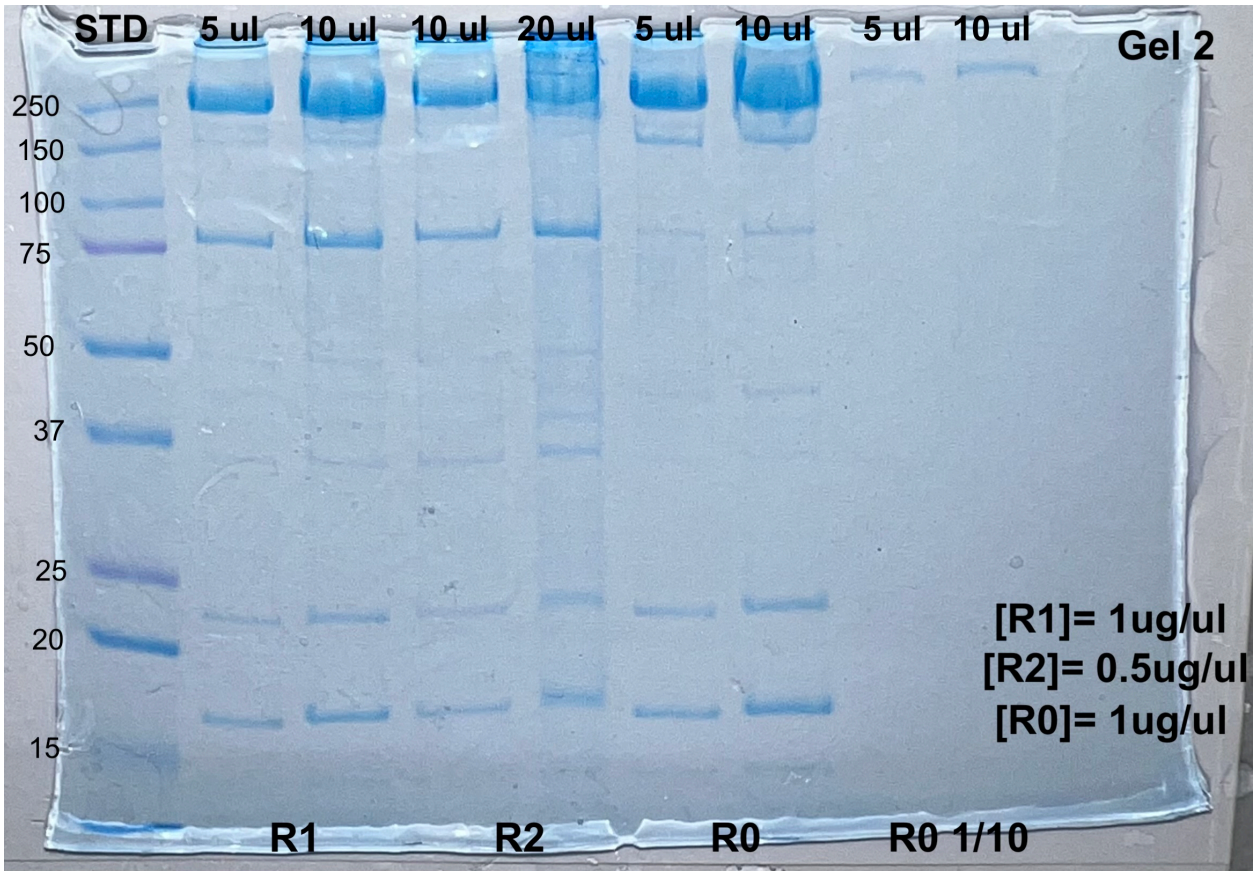

Supplemental Figure 1: Coomassie stain of purified rabbit myosin in gel-stain. Rabbit myosin was combined from three purifications.

R0= Rabbit 0 (purification #1); R1= Rabbit 1 (purification #2); R0 1/10= Rabbit 0 (purification #1-diluted to 1:10); STD= protein standard.

Appendix A: Myosin Purification Protocol

Protocol Provided by Dr. Leslie Anna Leinwand of University of Colorado Boulder, 2022

Note: The maximum yield is 1% of muscle weight

All procedures should be carried out in the cold room on ice

All equipment and solutions need to be precooled.

This prep is for 1 rabbit. Adding a second rabbit is feasible, though doing so adds a significant amount of solution volume (may be problematic during centrifugation steps) and time to the prep as a whole. Plan accordingly.

Day 1 (6-8 hours):

Prepared: Buffers A and B, 50 mls of 0.2 M EDTA. Coordinate centrifuge times for days 2 and 3.

Materials:

Large tray, Meat grinder, Blades, Scissors, Saran wrap, Large beaker with stir bar, Cold water jug, Bucket of ice.

Place all items in the cold room so that they are available at the start of the dissection. Add DTT and ATP to buffers A and B, as specified. Also place 2 liters of acetone in the cold room if planning on preparing acetone powder.

SKELETAL: Remove pectoralis muscle from a freshly killed rabbit, trying to remove the top layer of muscle as a whole. Wrap in Saran wrap and keep on ice. Remove the tendons and outer fascia from the muscle and chop the tissue into half- to quarter-inch pieces.

CARDIAC: Remove the left ventricle from freshly killed pig heart. Chop into half inch pieces.

Pass through a pre-chilled meat grinder that has been rinsed with **0.2 M EDTA**, collecting the ground tissue in a weigh boat. Re-grind and remove tissue from inside grinder.

Weigh tissue Wt. = _____ g

Add 2 ml of **buffer A** per gram of tissue.

1st volume added = _____ ml buffer A

Total volume: _____ ml

(e.g. tissue weight = 100g, 1st and total volume = 200 ml)

Stir gently with a large stir bar for **12 minutes**. The stirring time matters; do not let this mixture sit indefinitely.

Add an equal amount of cold ddH_2O quickly to stop the reaction.

2nd volume added = _____ ml cold ddH_2O

Total volume: _____ ml

(e.g. 1st vol. = 200 ml, 2nd vol. will equal 200 ml, total = 400 ml)

Add cold ddH_2O to dilute to half again (solution is now ¼ x).

3rd volume added = _____ ml cold ddH_2O

Total volume: _____ ml

(e.g. total was 400 ml, 3rd volume is 400 additional ml, total is now 800 ml = 4x 1st volume)

Filter through 4 layers of cheesecloth into a 4L beaker (a large graduated cylinder works well, too). Be prepared to change the cheesecloth if necessary.

Slowly add cold ddH_2O to precipitate the protein, diluting to a final concentration of 1/10.

1st volume added X 6 = _____ ml cold ddH_2O

Total volume: _____ ml

(e.g. 1st volume = 200 ml, x 6 = 1200 ml, + current 800 ml = 2000 ml = 10x original volume)

Add protease inhibitor cocktail. For BioVision Protease Inhibitor Cocktail (cat # K 271-500), dilute stock to 1x, add 1.5 **ul** per 500 **mls** of solution.

Cover and let the precipitate settle in the cold room. This step may take 3 to 4 hours, with the precipitate settling slowly at first, and then abruptly forming a layer at the bottom of the beaker. Check every 30 minutes or so. During this downtime, prepare **buffer C** and keep it in the cold room or refrigerator. This is also a good time to move on to the acetone powder prep using the pulp from the filter step (see "Preparation of Acetone Powder from Rabbit Skeletal Muscle").

After the precipitate has settled, siphon off as much clear liquid as possible. Be careful not to take any of the precipitate.

Centrifuge the precipitate in a SLA-3000 rotor (holds 6, 500 ml tubes) at 8,000 rpm (RCF = 10816 g) for 10 minutes at 4° C.

Discard the supernatant and soak the pellet in a minimal amount of **buffer B** while preparing for dialysis, then gently resuspend (solution should be thick).

Dialyze overnight against 4 L of **buffer C** at 4° C.

Day 2 (5-6 hours):

Materials:

Large beaker with stir bar, Cold ddH20 water jug, Bucket of ice, Centrifuge tubes (~ 25 ml. , Check compatibility with the rotor you intend to use), Medium graduated cylinder, Saran wrap.

Pour solution into a cold 600 ml beaker (solution should be cloudy). Estimate or use the graduated cylinder to determine the volume. Gently stir in the cold room while slowly adding an equal amount of cold ddH_2O.

Continue to stir for 30 minutes (precipitation of actomyosin).

Centrifuge in the ultracentrifuge rotor T-865 at 20,000 rpm for 1 hr at 4° C. Alternatively, use the Beckmann 50.2 Ti rotor and spin at 18,400 rpm (both = RCF ~41,000). Be sure you or someone doing the prep is fully trained in the use of the centrifuge, including cleanup and shutting down the machine.

Following the spin, the tubes should have a distinct pellet, a clear middle layer, and a cloudy layer of fat at the top of the tube. Remove the middle-layer supernatant (don't take the fat). You should expect to lose a sizeable portion of the volume you originally added to the tube. Dilute the supernatant with cold ddH_2O 10-fold (i.e. if 100 ml of supernatant, dilute to 1 L).

Cover and let sit for 3-4 hours in the cold room. A distinct layer should form, as in the Day 1 prep. Prepare **buffers D and E** as specified.

Siphon off clear supernatant and centrifuge the rest in SLA-3000 rotor at 8,000 rpm for 15 minutes at 4° C.

Soak and gently resuspend pellet in about 10 ml **buffer D.**

Dialyze overnight against 2 L **buffer E**, changing the buffer at least once if possible.

Day 3 (5 hours):

Materials:

50 ml beaker, Bucket of ice, 10 ml pipette(s), Saran wrap.

Remove the myosin from dialysis, saving a volume of buffer E to later determine protein concentration.

To clarify myosin, spin in the ultracentrifuge rotor T-865 at 20,000 (or 50.2 Ti at 18,400) rpm for 2 hrs at 4° C.

Using a transfer pipette, remove the myosin from the middle layer (leaving the upper fat layer).

Determine the concentration using 3 dilutions (1:25, 1:50, 1:100) and the following:

$((A_{280} - A_{320})/0.55)$ x dilution = _____ mg/ml

Dilute to 50% with cold glycerol by stirring in the cold room. Store at -20C

Buffers

*ATP and DTT are added the morning of the prep

Solutions should be pre-chilled.

Buffer A: Extraction Buffer 500 ml

0.3 M KCl	50 ml of 3 M KCl
0.15 M KPi	30.5 ml of 1 M K_2HPO_4
	44.35 ml of 1 M KH_2PO_4
20 mM EDTA	50 ml of 0.2 M EDTA
5 mM $MgCl_2$	510 µl of 4.9 M $MgCl_2$
*3.3 mM ATP	1 g ATP
pH to 6.7	
*5 mM DTT	2.5 ml of 1 M DTT, or 0.396 g
Qs to 500 ml	

Buffer B: Suspension Buffer 50 ml

1 M KCl	16.6 ml of 3 M KCl
60 mM KPi	1.5 ml of 1 M K_2HPO_4
	1.5 ml of 1 M KH_2PO_4
20 mM EDTA	5 ml of 0.2 M EDTA
pH to 6.7	
*5 mM DTT	250 µl of 1 M DTT
Qs to 50 ml	

Buffer C: Dialysis Buffer 4 L

0.6 M KCl	800 ml of 3 M KCl
25 mM KPi	40.8 ml of 1 M K_2HPO_4
	59.2 ml of 1 M KH_2PO_4
pH to 6.7	

*5 mM DTT		20 ml of 1 M DTT or 3.085 g
	Qs to 4 L	

Buffer D: Resuspension Buffer 21 ml

3 M KCl		20 ml of 3 M KCl
50 mM KPi		670 µl of 1 M K_2HPO_4
		330 µl of 1 M KH_2PO_4
	pH to 6.7	
*5 mM DTT		105 µl of 1 M DTT
	Qs to 21 ml	

Buffer E: Dialysis Buffer 2 L

0.6 M KCl		400 ml of 3 M KCl
50 mM KPi		58 ml of 1 M K_2HPO_4
		42 ml of 1 M KH_2PO_4
1 mM NaN_3		2 ml of 1 M NaN_3
	pH to 7.0	
*5 mM DTT		10 ml of 1M DTT
	Qs to 2 L	

Stocks

1 M NaN_3	MW = 65.01
0.65 g NaN_3	
Qs to 10 ml	

3 M KCl MW = 74.55

447.36 g KCl

2 ml of 1 M NaN_3

Qs to 2 L

1 M K_2HPO_4 MW = 174.18

34.84 g K_2HPO_4

200 µl of 1 M NaN_3

Qs to 200 ml

1 M KH_2PO_4 MW = 136.09

27.22 g KH_2PO_4

200 µl of 1 M NaN_3

Qs to 200 ml

1 M $MgCl_2$ MW = 203.3

2.03 g $MgCl_2$

10 µl of 1 M NaN_3

Qs to 10 ml

0.2 M EDTA MW = 292.2

11.69 g EDTA

200 µl of 1 M NaN_3

drip NaOH until dissolved

pH to 8.0

Qs to 200 ml

1 M DTT MW = 154.3

7.715 g DTT

50 µl of 1 M NaN_3

Qs to 50 ml

Protease Inhibitor Cocktail

American Bioanalytical cat# **AB11014**:

AEBSF, Pepstatin A, E-64, Bestatin,

Sodium EDTA

Cold ddH_2O

4 L